Additive Manufacturing of Titanium Alloys: Processability, Properties, and Applications

ADVANCED ENGINEERING MATERIALS
www.aem-journal.com

Additive Manufacturing of Titanium Alloys: Processability, Properties, and Applications

*Mohammad Hossein Mosallanejad, Ata Abdi, Farshid Karpasand, Navid Nassiri, Luca Iuliano, and Abdollah Saboori**

The restricted number of materials available for additive manufacturing (AM) technologies is a determining impediment to AM growing into sectors and providing supply chain relief. AM, in particular, is regarded as a trustworthy manufacturing technology to replace the traditional ones for Ti alloy components. Furthermore, the AM processability of Ti alloys and their features, such as microstructure, texture, and mechanical properties, is strongly dependent on the chemical composition of the processed alloy. It is essential to consider the ultimate applications as well. β Ti alloys are gaining popularity in the biomedical industry, while α + β Ti alloys are increasingly utilized for producing components in the automotive and aerospace sectors. Consequently, the topic has garnered considerable interest, and the current text reviews the advances during the last 10 years in this area to facilitate the pathway from the demanded Ti alloy to the best-fit AM procedure. While systematically reviewing the works published in the literature, the current text attempts to establish a link between the production method, feedstock type, chemical composition, and the ultimate application. This review also features practical applications of Ti components produced by metal AM methods and offers prospective possibilities and industrial applications.

1. Introduction

Additive manufacturing (AM) is a recent and promising manufacturing concept that is based on slicing a solid model into a predefined number of layers, defining a toolpath for each layer, transferring this data to the device, and developing the component layer-by-layer from the feedstock material—in the form of powder, wire, and sheet—using a heat source.[1,2] AM is featured with several promising advantages over conventional manufacturing methods like machining, forging, casting, and finishing; AM technology permits the design and production of complicated geometries in a near-net shape manner that would be challenging or impracticable to achieve via conventional methods. Besides, as opposed to traditional processes, AM significantly saves raw materials and uses no tools, minimizing production costs and energy. Last but not least, novel geometries now possible by AM technology can contribute to performance and ecosystem advantages in the employment of components, further adding to the sustainability of the method.[3–5] For example, AM may contribute to weight reduction in aviation industries by allowing redesigns for a vast number of parts, leading to greater aircraft fuel efficiency.[6,7] For further details, one may refer to Section 2, where various AM methods are explained. With considerable industrial benefits, metal additive printing offers a way to build optimized components. The insufficient capacity to provide supplies on request and the restricted quantity of materials accessible are barriers to development into other industries, such as the automotive sector, and to facilitating supply chain alleviation.

Titanium alloys, as revolutionary materials possessing unique corrosion, biomedical, and mechanical properties, are usually the first choice among the candidates for various applications such as biomedical implants,[8,9] high-temperature creep resistance,[10] and aerospace.[11] However, one major drawback of titanium alloys is that the alloy is not usually cost-effective.[12,13] Despite their popularity, the development of titanium alloys poses challenges due to the inherent difficulties associated with traditional manufacturing methods such as casting, rolling, and forging.[14] Titanium alloys have not been cast using the traditional method frequently due to the strong reactivity of liquid titanium with

M. H. Mosallanejad, L. Iuliano, A. Saboori
Integrated Additive Manufacturing Center (IAM)
Department of Management and Production Engineering
Politecnico di Torino
Corso Duca Degli Abruzzi 24, 10129 Torino, Italy
E-mail: abdollah.saboori@polito.it

A. Abdi
Faculty of Materials Science and Engineering
K.N. Toosi University of Technology
Tehran 19395-1999, Iran

F. Karpasand, N. Nassiri
Department of Materials Engineering
Science and Research Branch
Azad University
Tehran 1477893855, Iran

The ORCID identification number(s) for the author(s) of this article can be found under https://doi.org/10.1002/adem.202301122.

DOI: 10.1002/adem.202301122

mold sands.[15,16] Moreover, the low thermal conductivity of titanium alloys makes their machining inherently challenging and results in a high cutting temperature.[17] Additionally, the springback characteristics of these alloys make it difficult to form them at ambient temperature, even under annealed conditions.[18,19] As a result, industrial companies (e.g., GE Additive) are working on AM techniques to improve productivity and save costs while maintaining the distinctive advantages of titanium alloys.[20–22] Usually, titanium alloys are accessible in powder and wire form, making the alloy a suitable feedstock candidate for all main categories of metal AM.[23,24] As the title suggests, this review article will focus on the processability of common titanium alloys produced by different metal AM methods. Extensive research has been conducted in this field; the processing of Ti6Al4V alloy, the most popular titanium-based alloy, has received extensive attention.[25–33] In terms of processability, Nguyen et al.[34] reviewed the processability of Ti6Al4V by various AM methods, including electron beam melting (EBM), laser powder bed fusion (L-PBF), and directed energy deposition (DED) methods. L-PBF and DED methods exhibit comparable strength to the conventionally produced counterparts, up to 25% higher. In addition, Hui Jun Yi et al.[35] reported that the in-process controlled cooling rates of Ti6Al4V produced via wire arc additive manufacturing (WAAM) resulted in higher strength and hardness but lower elongation than the conventional sample. Additionally, Pellizzari et al.[36] conducted a review of the L-PBF processing of recently developed six beta titanium alloys, suggesting their potential suitability as alternative materials for biomedical and aerospace applications. Among them, Ti2448 (Ti–24Nb–4Zr–8Sn), the most typical of the Ti–Nb alloy system, showed a high relative density when a combination of high energy density and low laser scanning speed was employed.[37] In addition, due to the excellent weldability and heat treatability of Ti5553 (Ti–5Al–5V–5Mo–3Cr) alloy, it is possible to achieve a wide processing window and high relative density (99.95%) in L-PBF processed bulk samples by precisely defining the energy density parameter.[38,39] Lu et al.[40] recently processed TA15 (Ti–6.5Al–2Zr–1Mo–1V) via hot WAAM (HWAAM) and reported that the relatively high tensile strength of the part was due to solid solution and boundary strengthening mechanisms. Needless to mention that the AM processing of other Ti-based alloys such as Ti55511 (Ti–5Al–5Mo–5V–1Cr–1Fe),[41] Ti–6Al–2Zr–1Mo–1V (TA15),[42] Ti–13Nb–13Zr,[43] Ti2448 (Ti–24Nb–4Zr–8Sn),[44] TNTZ (Ti–35Nb–2Ta–3Zr),[45] TLM (Ti–25Nb–3Zr–3Mo–2Sn),[46] Ti–42Nb,[47] Ti–6Al–7Nb,[48] and Ti–21S[49] have also been reported in the literature which will be discussed in more detail in the following sections. For this study, the selection of titanium alloys was based on several key criteria. First, the alloys chosen needed to have practical applications in sectors such as aerospace, biomedical, and automotive industries to ensure that the study findings would have direct real-world implications. Second, to comprehensively evaluate the performance of titanium alloys, a diverse set of alloys with a wide range of compositions, including alpha, beta, near-alpha, and metastable beta types, were selected. This would allow for exploring different material behaviors. Finally, the selected alloys needed to be available in forms suitable for metal additive manufacturing processes, such as powder or wire feedstock.

Despite the research and developments in Ti alloys processing by the metal AM technologies over the past several years,[24,50–54] the lack of a comprehensive review article covering all processability elements, from commercial and metallurgical aspects, is felt. In pursuit of this objective, a novel approach is introduced to examine recent research on Ti–6Al–4V and newly processed Ti-based alloys encompassing near-α, α, near-β, α-β, β, and metastable β variants.

This research aims to provide a comprehensive overview of recent advances in titanium processing through metal additive manufacturing since 2014, addressing critical aspects related to the processability, mechanical properties, and microstructural evolution of various titanium alloys. By evaluating these factors under different conditions, including as-received, heat-treated (HT), and hot isostatic pressured (HIPed) states, this study seeks to bridge existing knowledge gaps. Additionally, the article explores the diversity of metal additive manufacturing methods (L-PBF, EBM, DED, WAAM) by commercial equipment manufacturers (Arcam AB, EOS, Concept Laser GE, Renishaw, SLM Solution, Realizer, Trumpf, Farsoon) to assess their applicability for processing the studied titanium alloys.

The choice of AM technologies was made based on their relevance to titanium alloy processing, capability to produce test specimens and representation of commonly used methods in the industry. The criteria for selecting AM technologies included their suitability for processing titanium alloys, as the study aimed to achieve this objective. EBM and L-PBF were selected because they are widely used in the aerospace and biomedical industries. DED and WAAM were chosen as emerging technologies with unique advantages, particularly in large-scale production. In addition, the availability of commercial-grade machines from notable manufacturers such as Arcam AB, EOS, Concept Laser GE, Renishaw, SLM Solution, Realizer, Trumpf, and Farsoon ensured that the study's results could be applied to practical applications.

Furthermore, this study examines the potential, challenges, and applications of titanium-based alloys across aerospace, biomedical, and automotive industries, offering valuable insights into their suitability for various sectors within the realm of additive manufacturing and future research directions.

2. Additive Manufacturing

AM technology, also known as 3D printing, refers to the manufacturing processes where a final component is developed additively, i.e., layer-by-layer, based on a solid digital shape. A computer controls the steps from the CAD model to AM works entirely. According to ISO-ASTM 52 900, AM is designated as the "process of joining materials to fabricate parts from 3D prototype data, customarily layer-by-layer, as objected to subtractive manufacturing and formative manufacturing methodologies".[55] AM technologies are divided into two major categories: direct and indirect methods. The direct AM technique integrates the forming and densification methods and produces finished components without needing postsintering. More specifically, direct AM utilizes a heat source, which has high energy intensity and can exert a large quantity of energy into a microscale-focused area, allowing it to process a wide variety of materials.[56] Compared to the indirect AM technique, the direct AM method can create parts with enhanced mechanical properties, higher

purity and density, and lower energy and time requirements. In indirect AM, initial three-dimensional structures are created using binder ingredients, followed by sintering the structure to remove the binder and densify the product.[57] Direct methods are self-divided into two distinctive groups: PBF and DED process. PBF method can be carried out using laser and electron beams as heat sources, introducing L-PBF and EBM methods, respectively.[58,59]

2.1. Direct AM Methods

2.1.1. L-PBF

L-PBF is one of the most significant direct AM processes, allowing the fabrication of objects with novel shapes and complicated interior structures.[60,61] As illustrated in **Figure 1**, from CAD data preparation until the disassembly of the produced part from the building platform, the L-PBF process comprises a sequence of steps. During the L-PBF methods, a thin layer of powder is spread on a base plate and then selectively melted according to the CAD data using a laser beam with a high energy density. Once the laser scanning is complete, the construction platform is lowered, allowing the next powder bed to be deposited and scanned by the laser beam. The procedure is repeated for consecutive powder layers until all essential components have been manufactured. Laser power, scanning speed, hatch spacing, and layer thickness are among the most determining process parameters in this method (**Figure 2**).[62,63] Meanwhile, various scanning strategies and process settings for different areas of the component and supports can be employed to create complicated structures.

Furthermore, L-PBF is characterized by rapid cycles of heating, melting, solidification, and cooling due to the employment of a highly focused laser beam with a fast-scanning speed. Experiencing very high cooling rates of up to $10^6 \frac{K}{s}$ results in a fine-grained structure and ultimately enhanced mechanical characteristics in L-PBF samples. On the contrary, large temperature gradients and layer-by-layer manufacturing lead to the production of L-PBF components with high anisotropic microstructure, residual stress, and random porosity distribution.[64]

In the L-PBF process, due to the prepositioned powders on the substrate, finer particles and lower energy input are required to create a fully dense part. This can be accomplished by employing higher scan rates and lower laser power.[54] Consequently, L-PBF is particularly notable for its exceptional precision and accuracy, making it the preferred choice for applications requiring intricate geometries and high surface quality. Its ability to work with a wide range of materials further enhances its versatility.[65]

2.1.2. EBM

EBM is another primary PBF method where an electron beam is employed as the heat source. This approach uses electric and

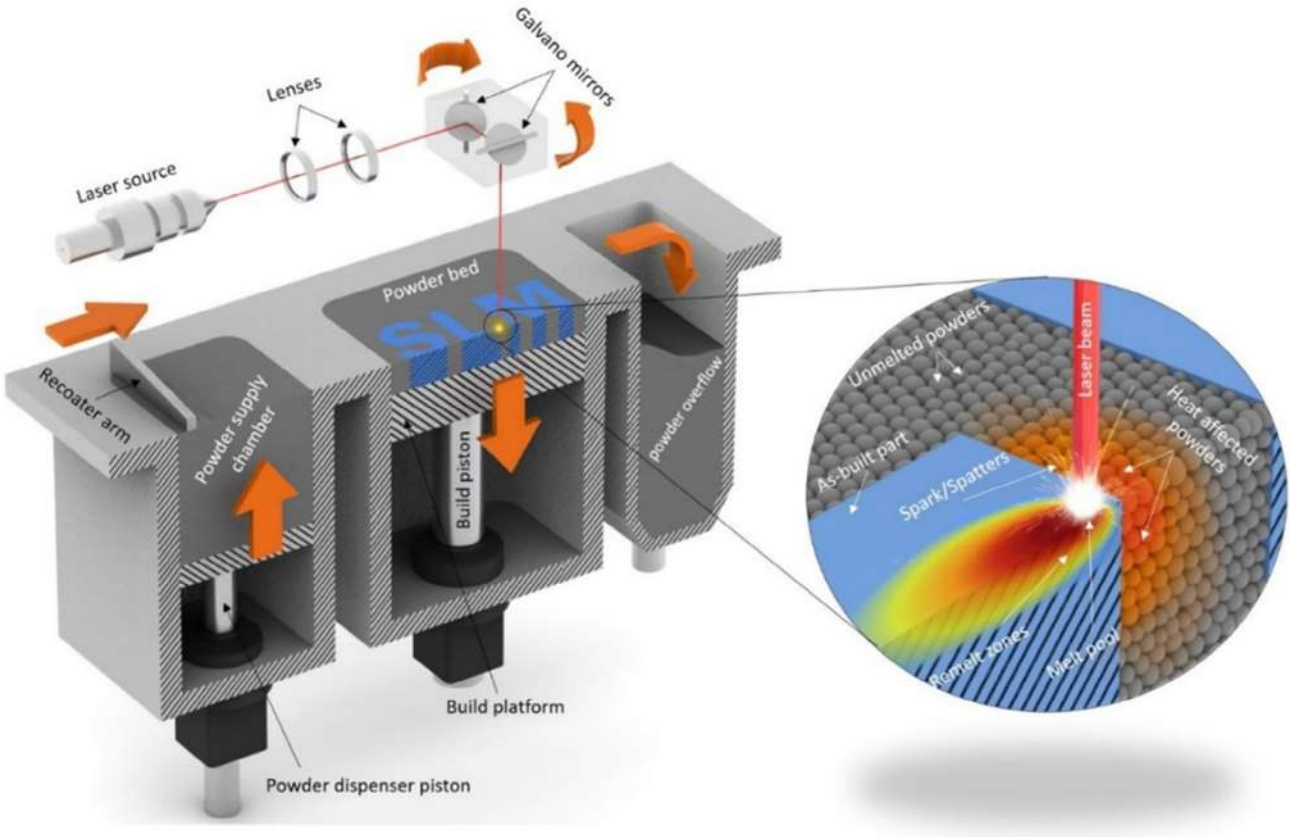

Figure 1. Schematic of L-PBF process.

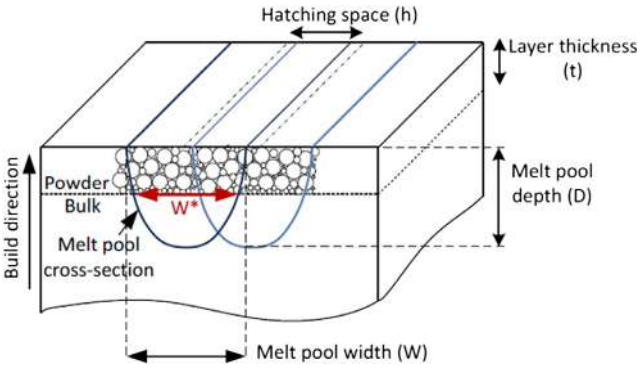

Figure 2. Schematic representation of the layer thickness, hatching distance, and melt pool characteristics. Reproduced with permission.[132] Copyright 2018, Elsevier.

magnetic fields to regulate and direct free electrons to form a focused beam under vacuum conditions. When an electron beam with a high velocity collides with a material, the kinetic energy is converted to heat. When concentrated, this high heat level is an effective way of melting electrically conducting materials. Because electrons scatter and disperse when they contact gas atoms between the electron gun and the substance being heated, EBM should be conducted in a vacuum chamber. The process proceeds via vacuum (10^{-4}–10^{-5} mbar), which is critical for metals and alloys with a high susceptibility to gases like oxygen and nitrogen.[66] Next, a slight helium pressure of 10^{-3} mbar is implemented to restrict electrostatic charging and smoke issues.[14,18] EBM offers unique capabilities and allows for producing closely stacked pieces in one printing job, which boosts the production rate. As depicted in **Figure 3**, a build file has been optimized, sliced, and uploaded into the EBM system. A powerful electron beam warms the powder bed to the ideal ambient temperature before melting the powder by contour melting and hatch melting, respectively. The built environment remains heated, sometimes reaching temperatures over 1000 °C, resulting in minimal residual stresses and permitting the processing of materials vulnerable to cracking. Moreover, because of the higher bed temperature in EBM, residual stresses are substantially lower than in L-PBF.

Notably, EBM distinguishes itself by its ability to produce components with exceptional material density and minimal internal stresses, rendering it highly advantageous for applications in aerospace and medicine. However, EBM may have limitations in dimensional accuracy and surface finish when compared to L-PBF. The selection between EBM and L-PBF depends on the specific needs of the application, with L-PBF excelling in intricate geometries and achieving high surface quality. At the same time, EBM is preferred for superior material quality and lower internal stresses.[67]

2.1.3. DED

DED is an AM method that relies on computer numerical control, adding flexibility to the method, material feeding, and welding. A laser beam, an electron beam, or an electric arc are

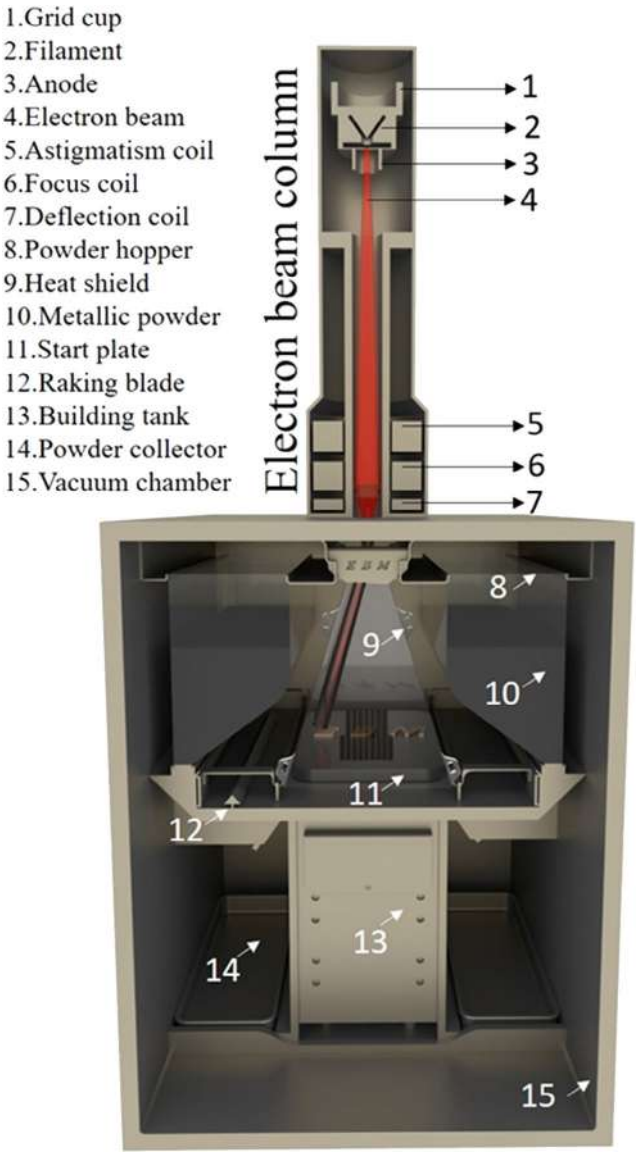

Figure 3. Principle schematic of EBM machine.

instances of thermal energy sources. In contrast, the metal components used as feedstock might either be wire or powder. Consequently, the commercially available different DED technologies include laser-based DED—also known as direct metal deposition which employs laser beam and metal powder, WAAM, and wire-feed electron beam additive manufacturing.[68,69] Instead of melting the metal particles in the powder bed, this process deposits the wire or powder into the molten pool formed when the heat source and the material interact (**Figure 4**). When a layer is completed, the nozzle or substrate shifts as much as the previous layer thickness to deposit the second layer.

As a result, a dense 3D shape with low porosity is generated. DED can be conducted in an inert chamber, too. The DED method is primarily utilized for the manufacture of near-net-shape objects that may require postmachining since it leads to a coarser surface than the PBF methods. Besides, this method

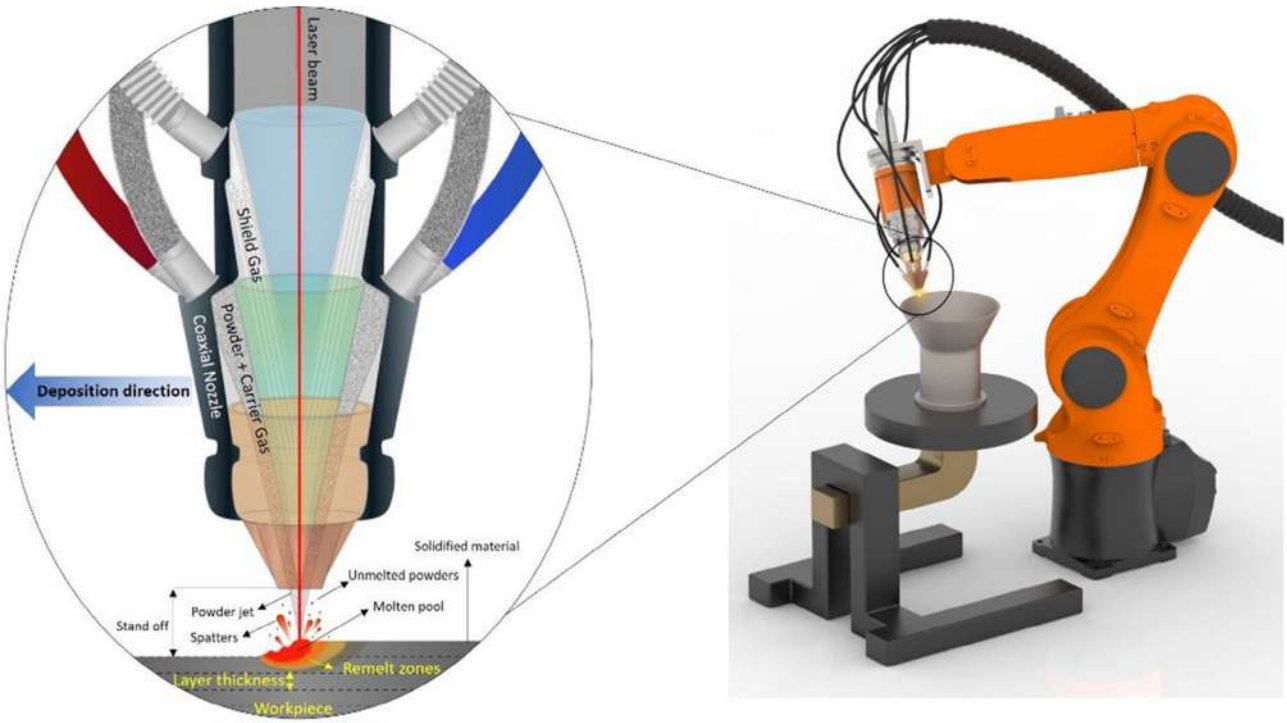

Figure 4. Schematic of DED technology.

can be employed to repair damaged industrial components with a complicated geometry.[36,70]

Also, the powder-based DED process involves the simultaneous delivery of feedstock powder and laser, necessitating a lower laser scan rate and greater laser power to guarantee that the melt pool is sufficiently large to accommodate and melt the metallic particles.[54] In contrast, the DED process, known for its material efficiency and scalability, is often employed in the production of large-scale structures and components. Its capacity to deposit material layer by layer while simultaneously fusing it with the existing structure makes it well-suited for applications where size, structural integrity, and material conservation are paramount.[71]

WAAM is a notable subset of DED technologies where an electric arc is used as the primary heat source for melting continuous wire feedstock material. This molten material is subsequently deposited with precision onto either a substrate or a preexisting layer, building the desired three-dimensional component layer-by-layer.[72] This method offers distinct advantages, particularly in its efficient use of wire feedstock, which is typically composed of the same material as the final component. The electric arc generates the necessary heat for wire melting, and the rapid solidification of the molten material ensures the formation of the desired shape. This level of control makes WAAM suitable for manufacturing large components. WAAM has garnered significant attention across industries such as aerospace and automotive due to its potential for cost-effective production of large, nearly net-shaped parts. Its ability to produce components with fewer defects and specific material properties adds value to the realm of additive manufacturing.[73,74]

2.2. Indirect Methods

In contrast to direct AM procedures, indirect AM methods utilize techniques that produce a provisional metal/polymer component for further manufacture. These methods often require a postsintering process to achieve the desired density level.

2.2.1. Binder Jetting Technology (BJT)

Powder particles are bonded together using a liquid agent in BJT to generate a semifinished part, i.e., a green part. A layer of powder is extended for every component layer via a counter-rotating roller. Subsequently, the liquid binding agent is ejected by an inkjet print head to the powder bed to build the layer 2D model. After each layer, the build stage is lowered, and the stages are regenerated to obtain capacity for the next layer. Needless to say, postsintering is required to obtain a high-density level. Several parameters, like postprocessing, AM parameters, raw material, and powder bed formation, directly affect the final properties of the desired material.[75] As an indirect AM method, BJT allows several possible benefits. For instance, besides having a comparatively high fabrication rate, this procedure operates nearly any powder feedstock, with a lenient restriction over the sphericity and size distribution, and consolidates functionally graded materials.[75]

2.2.2. Atomic Diffusion Additive Manufacturing (ADAM)

Bound powder extrusion (BPE), also known as ADAM, is an innovative arrival to the metal AM family. In contrast to other

AM methods, ADAM devices do not solely employ metal powder as the feedstock. Alternatively, the metal powder is bound together in waxy polymers to create metal-embedded polymeric filaments.[76] The outcome is a component that is significantly more reliable and straightforward to utilize than loose powder. For instance, BPE material can be touched by hand and does not demand loose powder machine protection standards. After printing, ADAM is followed by two main postprocessing stages: 1) dissolving the polymer in a washing machine and 2) sintering the washed sample in a furnace, which results in a dense product.[77] The ADAM approach also has the advantage of not requiring a laser or electron beam as a heat source, making the procedure significantly cheaper and easier to perform than the direct AM methods.[78]

3. Titanium Alloys Processability

Ti alloys are frequently produced by conventional techniques, such as powder metallurgy, forging, and casting. In addition, Ti alloys frequently need postfabrication processes, such as machining and heat treatments, to improve their characteristics and achieve properties.[79] Despite its outstanding properties, such as good corrosion/oxidation behavior at elevated or room temperatures and high strength-to-weight proportion, the Ti alloy fabrication involves several issues during the conventional manufacturing techniques. Therefore, in recent years, AM methods have been widely implemented to process various types of Ti alloys to achieve a combination of physical and mechanical properties.[80] Among the various metallic materials, titanium-based alloys have been produced and developed by AM since the first years of AM introduction. **Figure 5**a indicates that, among all the investigations or studies reviewed in the literature since 2014 that focused on AMed Ti-alloys, the majority (90%) of them specifically investigated or examined Ti6Al4V as the titanium alloy of interest approximately. In other words, Ti6Al4V was the most frequently studied or researched alloy within the AMed Ti-alloy family thanks to its superior corrosion resistance and high mechanical properties.[81–96] The remaining publications (10%) illustrated by Figure 5b–d deal with different titanium alloys produced by well-known AM methods such as L-PBF, EBM, DED, WAAM, and BJT which received considerable attention for some reasons that will be discussed in the subsequent sections.[36,97–110] It can be noticed that while

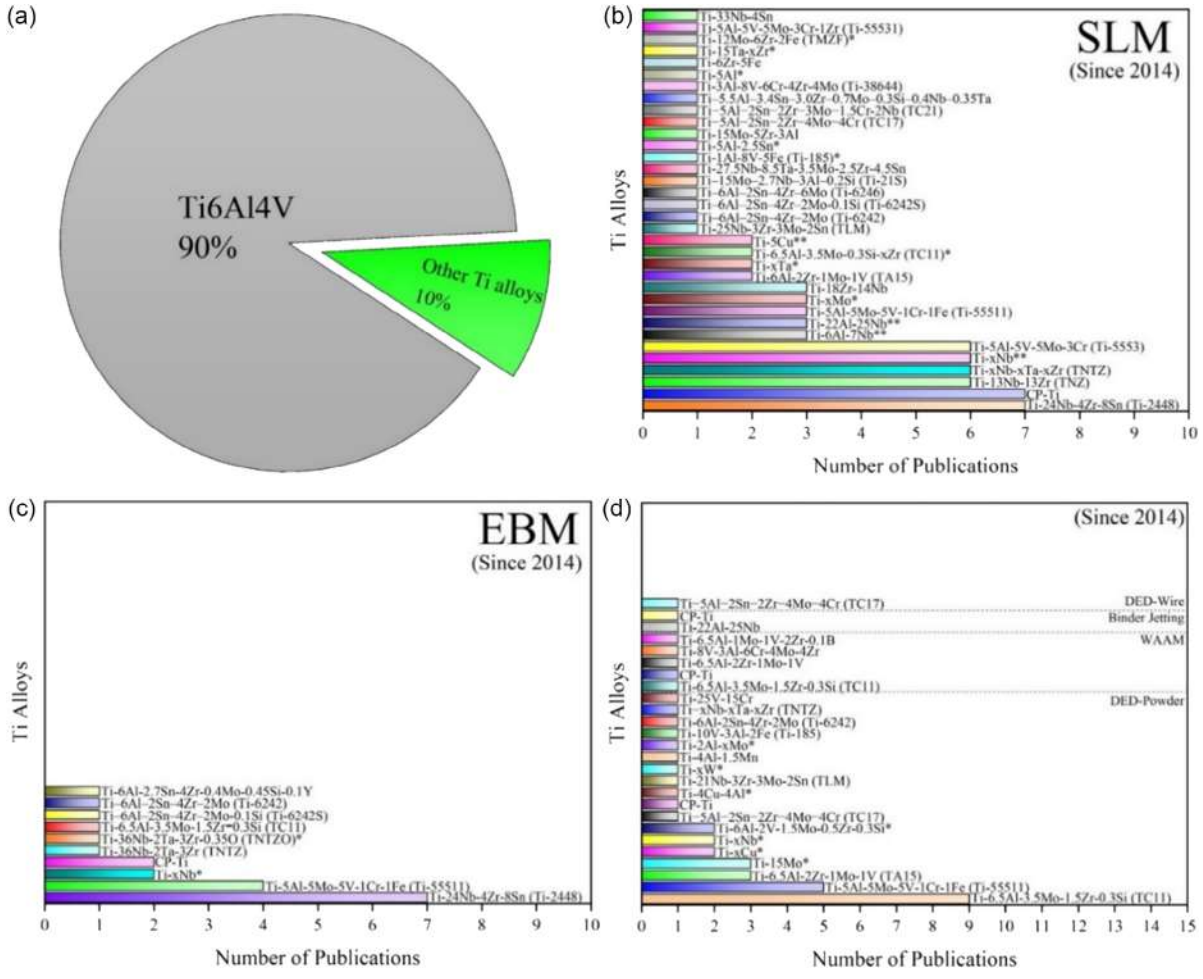

Figure 5. a) Wide range of Ti alloys produced by AM, b) number of publications by L-PBF method, c) EBM methods, and d) powder-based DED, WAAM, and BJT, database: Scopus.

Ti-2448 and commercially pure titanium (CP-Ti) have garnered the greatest interest in the L-PBF and EBM techniques, the TC-11 alloy has drawn the most interest in the DED method. The AM technologies involved in titanium-based are shown in **Figure 6**. It statistically shows the different machines employed for the works conducted via EBM and L-PBF methods. In the L-PBF method, the most common machines for alloy development are the EOS M270 and EOS M280, whereas the most frequent machines used in the EBM method are the Arcam A2 and Arcam A2X. As illustrated in Figure 6, the (*) mark highlights the alloys prepared via in situ alloying, with the alloys marked with (**) being developed by both in situ alloying and prealloy powders. Finally, alloys with no marks are all processed in prealloy condition.

3.1. Direct Methods

3.1.1. L-PBF

Numerous research works have been dedicated to the L-PBF process in recent years. The data on the average optimal mechanical properties for the L-PBF as-built samples extracted from the previous studies are compiled, and the summary is illustrated in **Figure 7**a. Additionally, the properties of the HIP and HT samples are demonstrated in Figure 7b. It is interesting to note that Ti6Al7Nb and TC11 alloys possess the highest ultimate stress (UTS) among alloys created using L-PBF without post-processing, such as HIP and HT, as illustrated in Figure 7a. However, Figure 7b demonstrates that the Ti6242 and Ti55531 alloys have the highest UTS after the HIP and HT processes.

In 2014, Simonelli et al.[111] explored the Ti6Al4V microstructure and mechanical anisotropy of as-built and stress-relived samples. To assess the influence of build orientation on tensile properties, the authors fabricated L-PBF specimens in three distinct orientations. They showed that defects in the microstructure, such as voids, were randomly distributed and not significantly affected by build orientation or distance from the build platform. They further noted that the α′ phase had a weak texture, while the prior-β grains possessed a strong (100) texture in the grain growth direction.

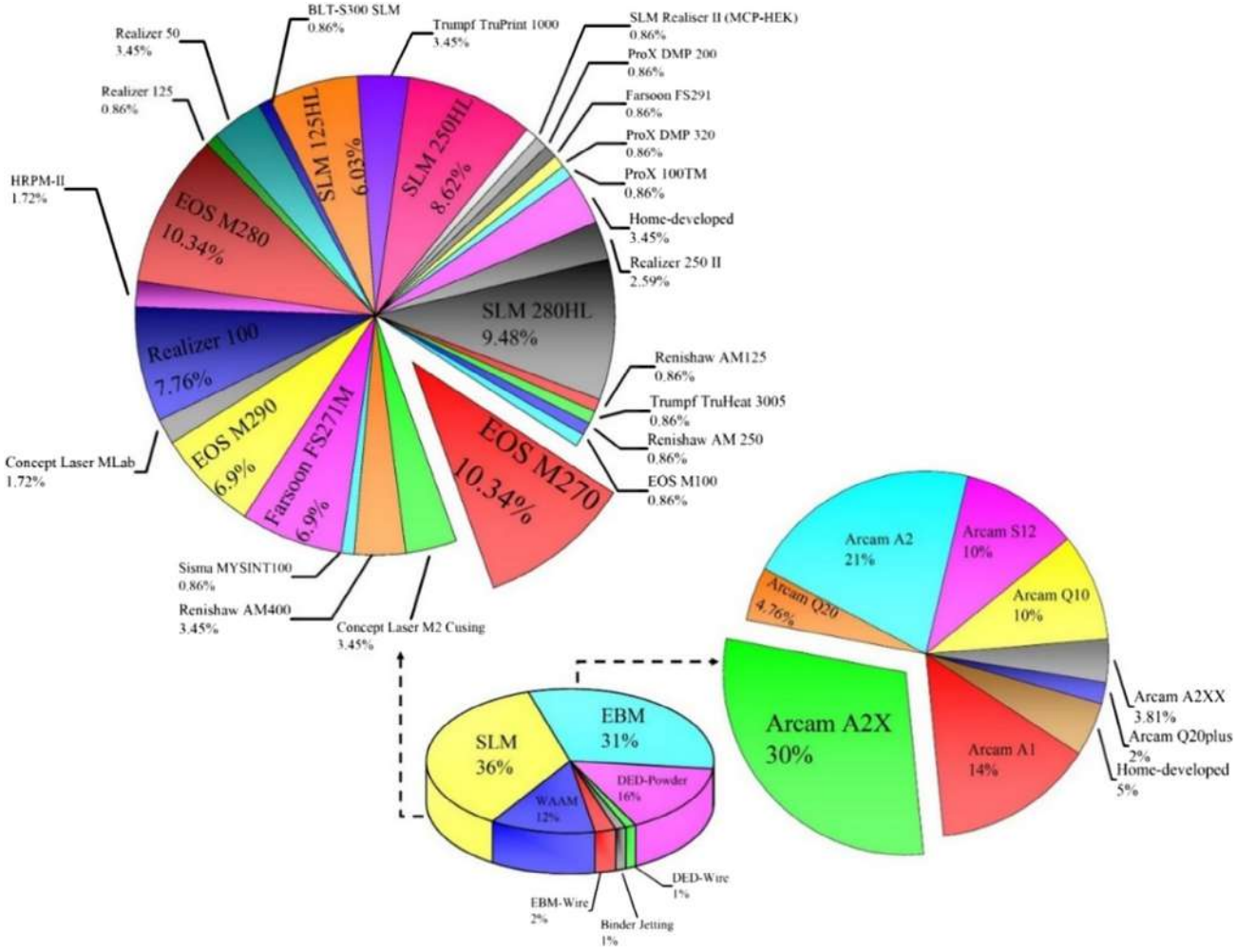

Figure 6. A statistical representation of titanium-based alloys produced by various AM processes and machines used in the EBM and L-PBF processes. The data are extracted from 172 AM studies on Ti6Al4V alloy since 2014, database: Scopus.

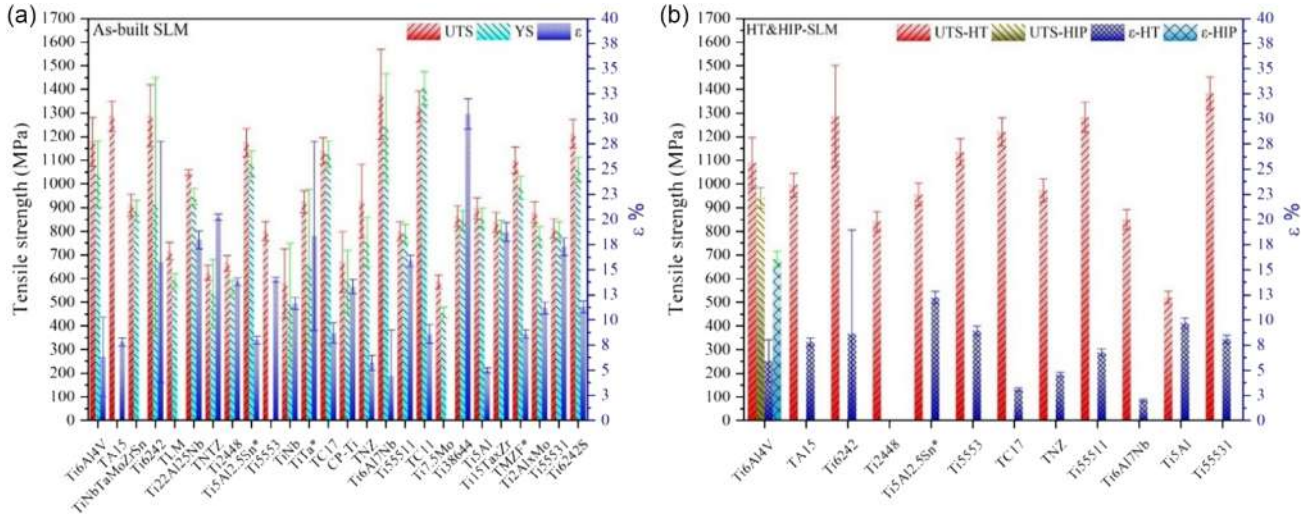

Figure 7. Average optimal tensile strength of alloys resulted by L-PBF methods, a) as-built, b) HT and HIP samples.

The ductility of specimens was found to be dependent on the build orientation, marking the impact of building orientation on the mechanical properties of the AMed sample by the L-PBF method (**Figure 8**a). In contrast, stress relief heat treatment was shown to enhance the ductility of the material and tensile properties with the build orientation influencing the sample behavior during the test (Figure 8b). Meanwhile, the fracture analysis indicated that all orientations exhibited rough and dimpled fracture surfaces, consistent with overload failures.

Kasperovich et al.[112] optimized both the process and posttreatment parameters of L-PBF Ti6Al4V samples, aimed at modifying the ductility and high cycle fatigue (HCF) strength associated with wrought Ti6AlV4. The α globular phase in an α + β matrix is seen in **Figure 9**a as expected for the wrought sample. In contrast, given its fast cooling rate, the L-PBF process induced an acicular martensite (α′) phase (Figure 9b). Moreover, as shown in Figure 9c, the primary fine martensitic formation is transformed into a combination of α and β phases by heat treatment at moderate temperatures, 700 °C, well below the β transus, in which tiny needle shapes of α were formed.

Figure 9c shows a coarsening of the microstructure, indicated by a more substantial column width. Heat treatment at 900 °C and HIP were employed to alter the microstructure into elongated grains embedded in the prior β matrix, as shown in Figure 9d,e. In addition, the authors reported that the tensile strength of the L-PBF sample was superior to that of the wrought one, even without any postheat treatments. Nevertheless, fatigue strengths and ductility were lower for the AMed samples, which were attributed to microcracks, unmolten particles, pores, and an

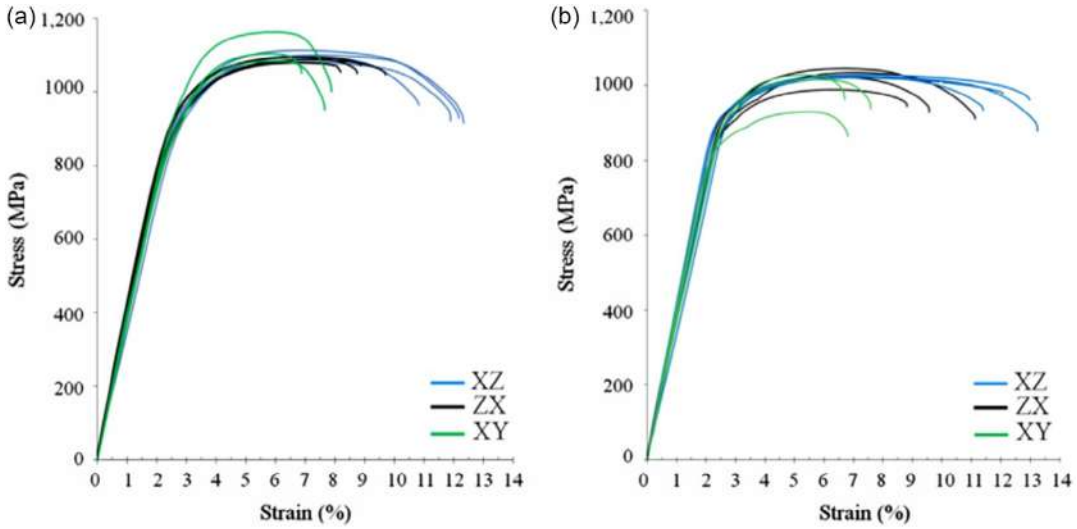

Figure 8. Stress–strain curves of the a) as-built and b) stress-relieved components. The differently colored curves represent the orientation in which the tensile bars were built, specifically the edge xz-orientation, vertical zx-orientation, and flat xy-orientation. Reproduced with permission.[111] Copyright 2014, Elsevier.

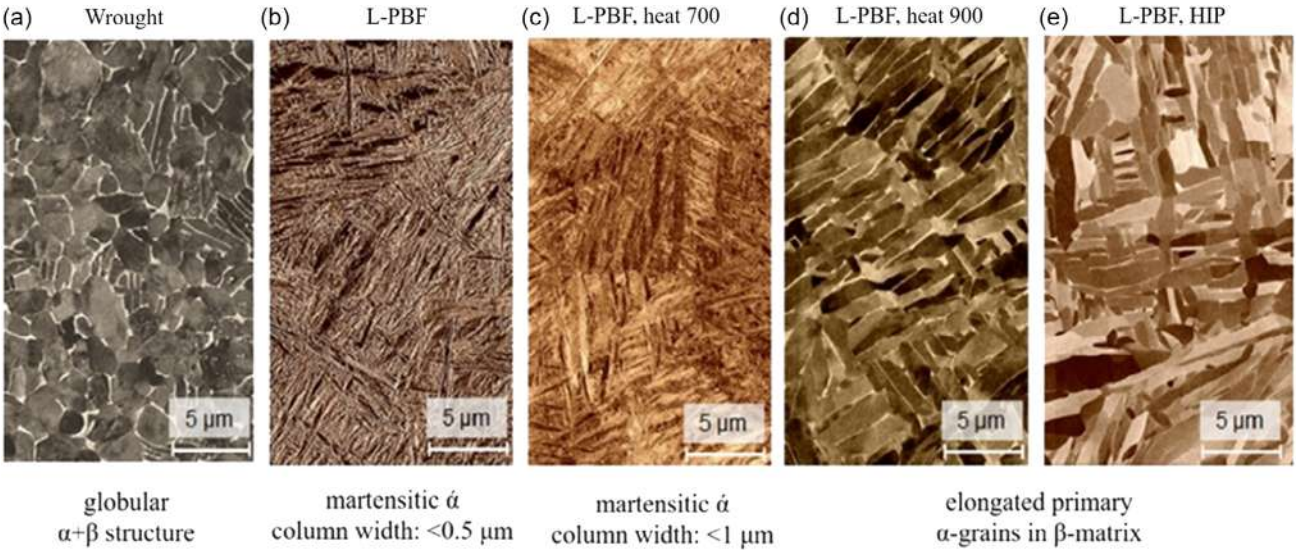

Figure 9. SEM micrographs of a) wrought sample, b) L-PBF as-built, c) L-PBF sample + HT at 700 °C, d) L-PBF sample + HT at 900 °C, and e) L-PBF + HIP. Reproduced with permission.[112] Copyright 2015, Elsevier.

undesirable martensitic microstructure. That being said, heat treatment did not contribute to a notable enhancement of HCF strength and ductility since inherent imperfections still remained. However, the authors reported HIP as profoundly contributing to improving fatigue strength and ductility by reducing porosity, marking the critical importance of HIP for cyclically loaded parts and improving ductility by up to 19.4%.

Ti6Al4V alloy, often applied as implants, is known to release aluminum and vanadium, both of which might cause biological issues.

Furthermore, the alloy's higher modulus compared to the patient's bone could potentially lead to stress shielding. Hence, attempts are made to introduce alternatives for the commonly used Ti6Al4V alloy. Metastable β-type titanium alloys have garnered significant attention as biomedical materials due to their exceptional corrosion resistance, excellent biocompatibility, superelasticity, shape-memory capabilities, and low elastic modulus. For instance, the Ti–13Nb–13Zr, a near β alloy, has attracted significant attention due to its low elastic modulus and nontoxicity, making it a desired alternative to Ti6Al4V specifically for biomedical applications. Zhou et al.[113] investigated the mechanical performance and microstructure of Ti–13Nb–13Zr alloy fabricated by L-PBF, followed by different postheat treatments. They reported morphological transformations of prior β grains, which occurred via strain-induced grain boundary migration mechanism upon supertransus heat treatment. It was also reported that the columnar β grains' direction toward the building orientation would not change while the samples were heat treated in the subtransus temperature. The authors reported the formation of ω structure upon the water quenching process, citing local transformation of the original stacking sequence from…ABCABC… to a new stacking sequence …AB'AB'.

Ti–24Nb–4Zr–8Sn (Ti2448) is another β titanium alloy that has attracted considerable attention, particularly for its medical applications. Zhang et al.[114] investigated the influence of laser point distance and laser scan rate on the microstructure of L-PBFed low-modulus Ti2448 alloy. It was observed that reducing the laser scan speed would increase the density and microhardness, which can be attributed to a higher laser energy density. **Figure 10** exhibits the microstructure of specimens fabricated using laser distances of 40 and 100 μm and different laser scan rates. The combination of process parameters yielded low density (82–85%) at higher scan rates—Figure 10c,d, and near total density (>99.5%) at lower scan rates—Figure 10a,b. The report by L.C. Zhang et al.[114] emphasizes the critical role of scan rate in terms of modulating the laser energy density as compared with the laser point distance.

Other low-modulus, biocompatible β-Ti alloys with nonallergic elements like Ti–Nb–Ta–Zr (TNTZ) are also investigated and developed as candidates for new-generation implant materials.[115] Hafeez et al.[102] examined the superelastic behavior of porous, low-modulus β Ti–35Nb–2Ta–3Zr scaffolds having different pore dimensions produced using the L-PBF method. The samples are schematically shown in **Figure 11**. The superelastic properties and strain recovery through deformation were reportedly affected by the scaffold's pore size. Loading–unloading experiments with a 3% strain revealed that increasing the pore size led to a higher elastic strain and Young's modulus. Furthermore, the residual strain of components with different pore sizes showed that the recovered strain was approximately zero.

Schulze et al.[103] studied the mechanical properties of Ti–42Nb produced using the L-PBF method. As-printed bulk parts had a relative density of above 99.5% and were featured with microstructures having a uniform distribution of Ti and Nb. The product had a Young modulus of 60.51 ± 3.92 GPa and an ultimate tensile strength of 683.17 ± 16.67 MPa, making it a suitable candidate for orthopedic and dental implants.

Tantalum has been considered an attractive alloying element in titanium for biomedical purposes thanks to its good

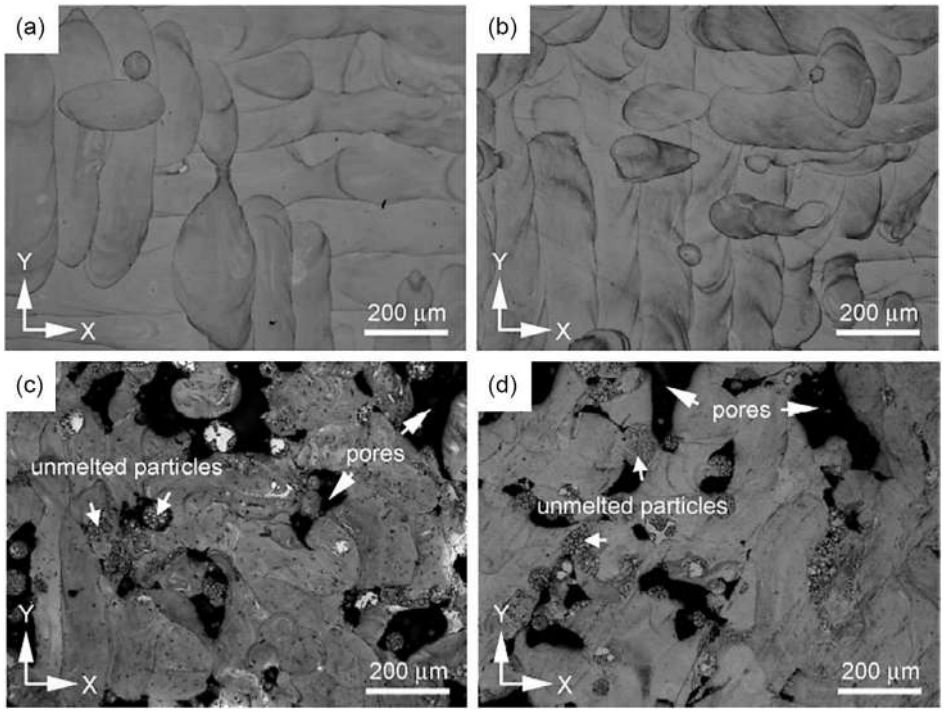

Figure 10. Optical microstructures of the as-built Ti–24Nb–4Zr–8Sn segments: a) $d = 40\,\mu m$, $v = 500\,mm\,s^{-1}$, b) $d = 100\,\mu m$, $v = 500\,mm\,s^{-1}$, c) $d = 40\,\mu m$, $v = 2000\,mm\,s^{-1}$, and d) $d = 100\,\mu m$, $v = 1667\,mm\,s^{-1}$. Reproduced with permission.[114] Copyright 2012, Scientific.Net.

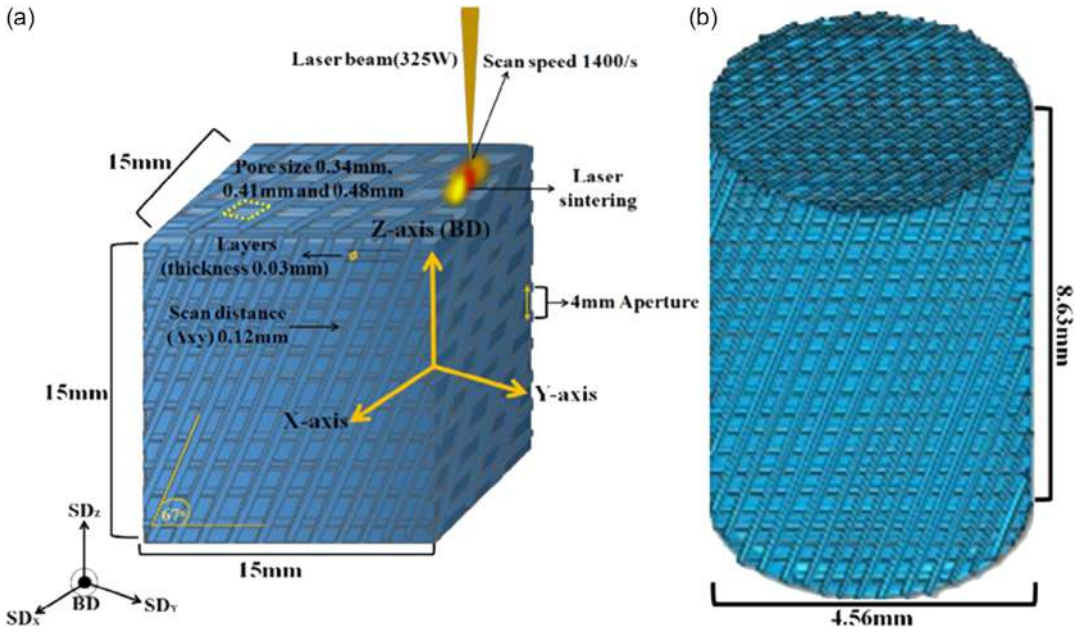

Figure 11. a) Layout of L-PBF-fabricated Ti–35Nb–2Ta–3Zr alloy and b) cylindrical specimens for mechanical measurement. Reproduced with permission.[102] Copyright 2020, Elsevier.

mechanical properties, high corrosion behavior, and biocompatibility. Besides, concerning the low cost and proper strength-to-density ratio, titanium tantalum (TiTa) alloys are a decent choice for medical purposes. Sing et al.[116] proved the ability to produce TiTa alloy through L-PBF. They observed that the TiTa alloy included only the beta phase due to the tantalum phase, which is stabilized by rapid solidification. Dispersed tantalum particles were observed in the fully melted TiTa matrix, resulting from

inadequate melting of the larger tantalum particles. TiTa components, compared to CP-Ti and Ti6Al4V segments, exhibited a combination of lower Young modulus (75.77 ± 4.04 GPa) and high strength (924.64 ± 9.06 MPa).

Ti–6Al–7Nb alloy, another Ti-based implant material, is an attempt to replace the contentious vanadium with niobium. This composition change has reportedly led to more desirable mechanical and corrosion properties than Ti–6Al–4V. In 2011, Chlebus et al.[117] studied the mechanical behavior and microstructure of the Ti–6Al–7Nb compound generated by L-PBF. It was demonstrated that samples contained a microstructure layered with tiny plates of α' martensite, hardened by a uniformly dispersed phase, likely β-AlNbTi2, giving the alloy high tensile and compressive mechanical properties. Though the produced sample ductility was very low, its mechanical properties significantly surpassed those obtained by conventional methods. However, postthermal treatment was found to be necessary to achieve the desired mechanical properties in light of the defects.

Ti–25Nb–3Zr–3Mo–2Sn (TLM alloy) features low elastic modulus and high strength. In 2019, Liu et al.[118] developed TLM alloy by L-PBF and compared it to the hot-rolled condition. Despite the strong texture observed in the L-PBFed specimen, it showed a higher ductility than the samples obtained for the hot-roll samples induced by martensite transformation. Actually, the martensitic transformation nucleation was impeded in the L-PBFed specimen thanks to the strong texture, high density of refined columnar grains, and subgrain boundaries, delaying the transformation-induced plasticity (TRIP) effects ($\beta \rightarrow \alpha''$), which can result in higher yield strength in the L-PBFed TLM samples.

Ti–15Mo–2.7Nb–3Al–0.2Si is another β-type alloy frequently compared with Ti6Al4V for use in biomedical and aerospace applications.[119] Pellizzari et al.[36] used L-PBF in 2020 to produce the Ti-21S alloy to evaluate the possible implementation of the Ti–15Mo–2.7Nb–3Al–0.2Si alloy for biomedical utilization. The top and the cross-sectional illustration of the microstructure material highlight a near-fully dense sample, as shown in **Figure 12**a,b, which also presents the formation of a columnar structure located adjacent to the building orientation. Additionally, the planar growth at the pool boundary turned into cellular inside the melt pool, as shown in Figure 12c, because of the constitutional undercooling formed ahead of the solid/liquid interface during solidification. Consequently, outstanding mechanical properties may be achieved in the as-fabricated state. Moreover, the authors claimed that the obtained Young's modulus was one of the lowest described in the report for this alloy type (52 ± 0.3 GPa), and mechanical strength was slightly lower than that of Ti6Al4V.

It is generally perceived that metal degradation in the human body owing to corrosion and wear is inevitable. In contrast, it is principally demonstrated that high amounts of dissolved metal ions in the body can provoke diseases such as cancer and allergies. Nevertheless, metals like Zn, Cu, and Ag demonstrate antibacterial features when added to biomaterial alloys. In 2018, Qin et al.[120] adopted L-PBF technology to investigate the heat

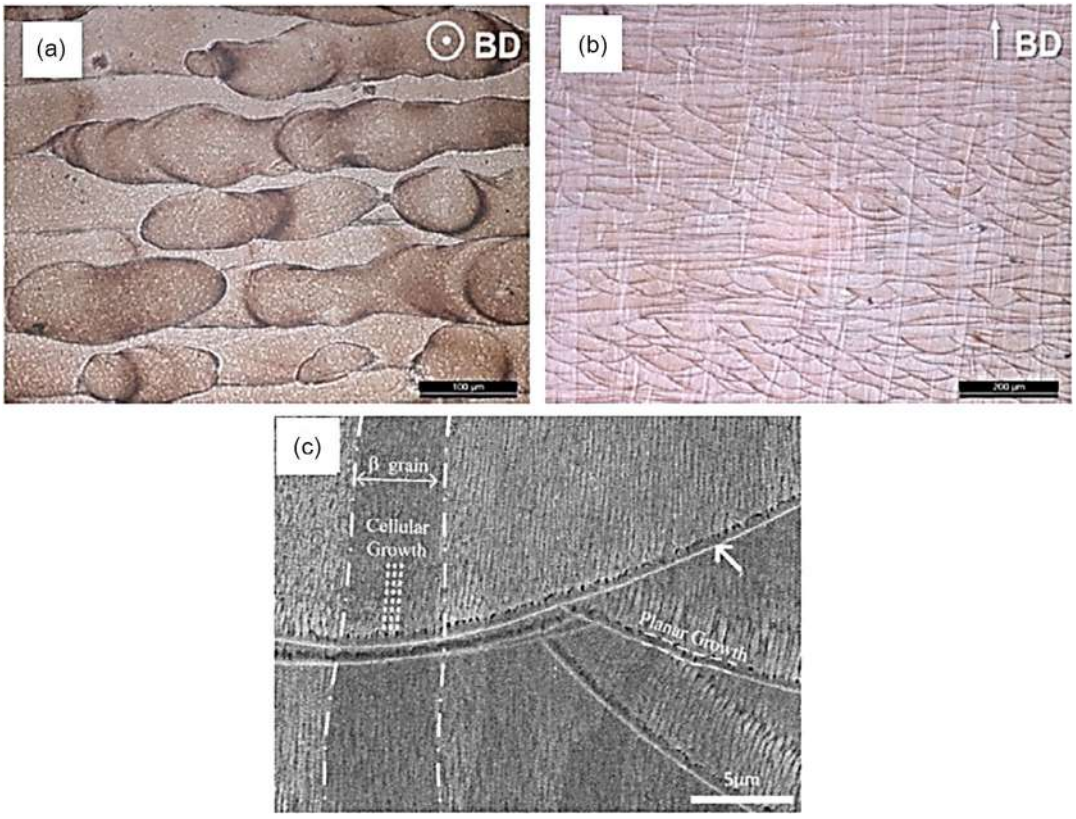

Figure 12. Cross-section of as-fabricated β-Ti21S; a) top, b) side sections, and c) transition of growth mechanism from planar, at the melt pool boundary, to cellular, inside the melt pool. Reproduced under the terms of the CC BY license.[36] Copyright 2020, MDPI.

treatment effect on an antimicrobial Ti–5Cu alloy and its corrosion behavior. It was observed that heat treatment could improve the distribution of the Ti_2Cu phase found in the as-built Ti–5Cu alloy and that the Ti_2Cu phase formation relied on the cooling rate following heat treatment. Unmolten Ti particles were reported in the as-built state after L-PBF of a Ti-Cu elemental mixture, which would deteriorate the final corrosion behavior.[121]

The near-beta alloy Ti–5Al–5V–5Mo–3Cr (Ti-5553) is well-suited for structural and aerospace applications due to its favorable mechanical properties and low density. Schwab et al.[38] examined the mechanical properties and microstructure of Ti-5553 prepared by L-PBF using a chessboard and striped hatch strategy, where a more than 99% density was reported. **Figure 13** illustrates the microstructure of the specimens, where nose-shaped to ball-shaped thick white lines resemble the melt pool boundaries after solidification. However, vertically generated grain boundaries can be recognized as thin white lines, and grains with a size of up to several 100 μm have grown near the melt pool boundaries. These

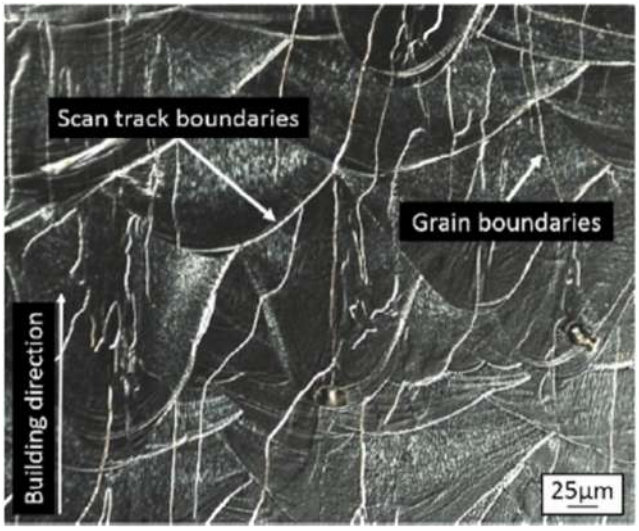

Figure 13. The microstructure of the part illustrates grain boundaries and scan track boundaries. Reproduced with permission.[38] Copyright 2016, Elsevier.

elongated grains with a high aspect ratio are grown in the building orientation, as depicted in **Figure** 13 and **14**a. Inside the melt tracks, however, the cross-sectional view indicates clusters of smaller grains, as shown in Figure 14b. Overall, the grains presented considerably irregular shapes. Furthermore, the authors reported that the specimens presented a maximum elongation of nearly 14% and an ultimate tensile strength of about 800 MPa.

High-performance titanium-based alloy Ti–22Al–25Nb is a lightweight intermetallic with numerous properties such as high-temperature resistance despite having a density of solely 60% of Ni-based superalloys, making the alloy suitable for high-temperature services approximately at 600–750 °C. In 2020, Zhou et al.[108] fabricated Ti–22Al–25Nb intermetallic by L-PBF and examined hatch distances of 0.08, 0.12, 0.16, and 0.20 mm. While a low hatching distance causes track overlap, surface roughness, excess energy input, and therefore the formation of gas pores, a high hatching distance results in poor part density due to the high viscosity of Ti–22Al–25Nb melt and hence a lack of appropriate gap filling. The effect of this behavior on the sample mechanical properties is demonstrated in **Figure 15**a. The enhanced mechanical properties at a hatching distance of 0.16 mm were attributed to high-density dislocation, favorable phase features, and high relative density at this parameter. Furthermore, the authors used the optimized parameters to demonstrate the method's capability for producing complex geometries, such as those used in microturbine engines (Figure 15b).

The Ti–5Al–5Mo–5V–1Cr–1Fe (Ti-55 511), a near-β titanium alloy, has a wide variety of applications. Following suitable heat treatments, its fatigue limit and strength can be enhanced up to over 800 and 1300 MPa, respectively. Therefore, this composition has been employed for plenty of aviation purposes, such as load-bearing parts, landing gears, and frames.[122] In 2020, Maimaitiyili et al.[123] examined Ti-55 511 processed via the L-PBF and EBM methods. It was demonstrated that both processes could produce Ti55511 and attain virtually full density with limited porosity. However, the L-PBF process was shown to produce a slightly lower density and more desirable surface condition. The shape of the pores in the EBM was mostly spherical, while more random shapes were noted in the L-PBF specimen. The dominant β phase in the feedstock powder became a

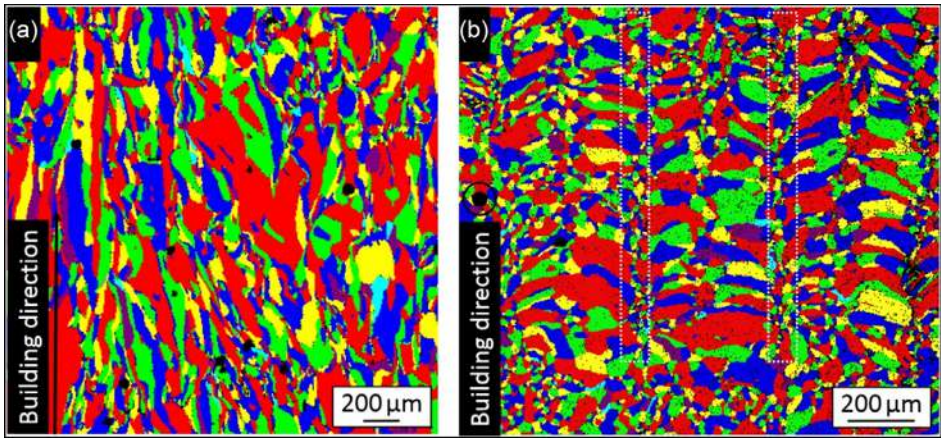

Figure 14. a,b) Cubic part grains in the longitudinal and cross-sectional cut. Reproduced with permission.[38] Copyright 2016, Elsevier.

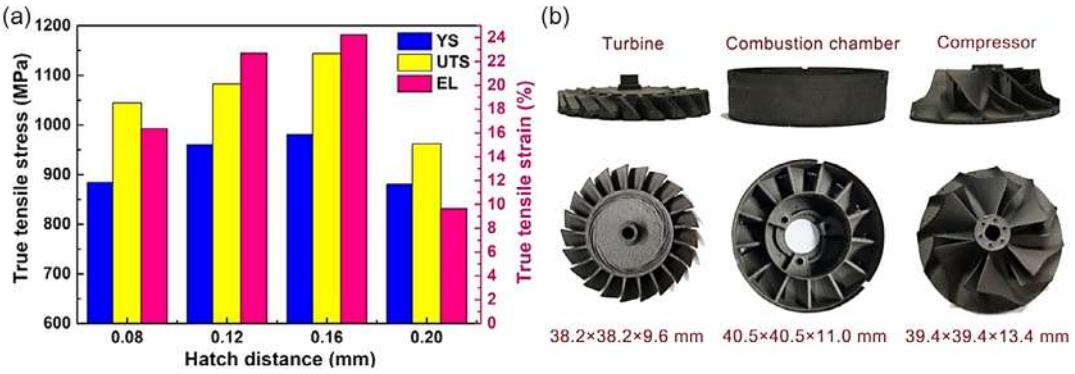

Figure 15. a) Variation of Ti–22Al–25Nb mechanical properties with hatch distance and b) capability of L-PBF for fabricating complex-shape parts out of Ti–22Al–25Nb intermetallic. Reproduced with permission.[108] Copyright 2020, Elsevier.

minority phase after EBM processing, while no phase transformation in the L-PBF parts was observed. The EBM specimens exhibited a lamella and Widmanstätten-like structure due to the high build temperature and comparatively slow cooling rate. The EBM parts showed about 10% higher microhardness than the L-PBF samples due to the lamella microstructure.

The near-α titanium alloy Ti–6Al–2Sn–4Zr–2Mo (Ti-6242) was fabricated a few decades ago for high-temperature applications. For instance, Ti-6242 is suitable for the aerospace industry for its excellent mechanical capability compared to Ti6Al4V at high temperatures. While Sn is regularly added to Ti for solution strengthening and is less influential as an α stabilizer, aluminum is a practical α-stabilizing element in Ti-6242.[124] Furthermore, to reduce the β-transus (T_β), molybdenum acts as a primary β-stabilizing element. Zirconium was initially intended to hinder the transformation rate of $\alpha \rightarrow \beta$ as an α stabilizer.

Consequently, it was re-evaluated as a solid solution strengthener with an inert effect on stabilizing phases.[125] In 2020, Fan et al.[126] employed L-PBF to develop Ti6242 alloy for the first time and achieved a crack-free microstructure with 99.5% density. Compared to the traditional lamellar structure, the L-PBF parts of Ti-6242 presented a martensitic microstructure with a weak texture. The 5% ductility of samples was principally owed to the unparalleled nanotwinned structure built during the L-PBF complex thermal cycles. The as-fabricated specimen was additionally strengthened by utilizing direct aging but at the cost of ductility reduction, reaching a high strength of 1510 MPa. There are also other research works[127–129] on the L-PBF of Ti-6242, detailing which are beyond the capacity of the current text. Lantaffi et al.[130] evaluated the build environment effects on the microstructural features of Ti-6242 alloy produced via DED. The amount of oxygen absorbed from the atmosphere during localized shielding gas processing inverted the Marangoni flow, altering the molten pool geometry and significantly impacting defect formation. Also, Chen et al.[131] deeply investigated defect formation using in situ synchrotron X-ray imaging. Laser power and traverse speed were reported to affect the building efficiency and lack of fusion regions. The authors reported that the pores were not engulfed at the solidification front because the interface had a cellular solidification mode (**Figure 16**), as expected during the DED of titanium alloys.

In 2017, Kreitcberg et al.[132] produced a new biomedical near-beta Ti–Zr–Nb compound using a combination of hatching distances, scanning speeds, and laser powers. The authors observed that the hardness and density of the Ti–18Zr–14Nb alloy increased with the energy, reaching its peak at 10–50 $cm^3\,h^{-1}$ build rate scales and a 25–45 $J\,mm^{-3}$ energy density. Higher build rates were gained in this processing phase at the cost of a rough surface finish. The Ti–Zr–Nb alloy built by this method was characterized to have superelastic and shape memory effect thanks to postprocessing heat treatment at 500 °C (30 min) followed by water quenching.

Alabort et al.[133] reported in 2020 the development of Ti–27.5Nb–8.5Ta–3.5Mo–2.5Zr–4.5Sn, a near-β titanium alloy optimum for AM with reduced stiffness and enhanced biocompatibility via the L-PBF method. Under an optimal manufacturing regime, this unique alloy presented a yield strength of 900 MPa, a strain-to-failure of 13%, and an elastic modulus of 65 GPa. While the elastic modulus of Ti–27.5Nb–8.5Ta–3.5Mo–2.5Zr–4.5Sn alloy was considerably lower (50%) than that of Ti6Al4V, its strength was solely 10% lower than Ti6Al4V; making the alloy a proper candidate for biomedical utilization.

Ti–1Al–8 V–5Fe (Ti-185) and other β -Ti compositions containing Fe are prevalent due to their low cost and suitable strength. However, when conventional processing methods are applied, the alloy may develop unwanted phases. This behavior is

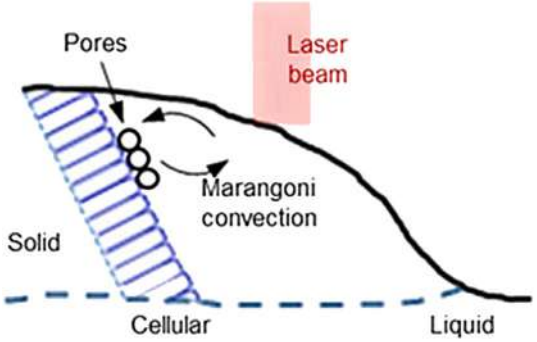

Figure 16. Schematic representation of pore pushing mechanism during the DED process of Ti-6242. Reproduced with permission.[131] Copyright 2021, Elsevier.

attributed to solid microsegregation of Fe, which occurs during casting, producing significant compositional variations and leading to the precipitation of brittle phases. Hence, to achieve a nanoscale distribution of α precipitates inside the β grains and a matrix with initial α phases at the grain boundaries, it is necessary to perform heat treatment.[134] In 2018, Azizi et al.[135] successfully produced Ti–Al–V–Fe samples using the L-PBF process. An exceptional combination of plasticity and strength was reportedly obtained due to a nanoscale alpha phase dispersed inside the β matrix, high dislocation density, and high oxygen content, which created solid solution strengthening and the formation of fine grains.

Titanium α alloys often display, more excellent resistance to high-temperature creep than α/β or β alloys, while α alloys show negligible heat treatment strengthening. Typically, these alloys undergo recrystallization or annealing to alleviate the stresses introduced during cold working. Compared to α/β or β alloys, they have often less forgeability but have high weldability. Near-α titanium alloy Ti–6Al–2Zr–1Mo–1V (TA15) is broadly utilized to create entire parts with asymmetrical geometries for aerospace applications.[136] Furthermore, the average strength of this composition at both high and room temperatures indicates it is suitable for creating nacelle center beam frames and bulkheads.[137] Cai et al.[138] developed TA15 components with a good combination of ductility and tensile strength by optimizing AM parameters and subsequent heat treatments. They observed that the specimen with 230 W laser power and 675 mm s^{-1} laser scan rate had the greatest tensile strength and elongation combination than other optimized parameter samples, which resulted from the joint influence of metallurgical quality, martensitic structure, and relative density. Moreover, a trivial reduction in the room and high-temperature tensile strength states was noticed when the layer thickness was increased from 30 to 60 μm, while the other processing parameters were kept constant. Additionally, under three indicative temperature scales, the authors observed transformations upon performing heat treatment:

Fine lath-like (α + β) with needle-like α′ martensitic phase → full lath-like (α + β) → coarse lamellar (α + β) with lath-like (α + β).

The Ti–5Al–2.5Sn, an α titanium alloy, demonstrates a high service temperature of 480 °C, outstanding weldability, average producibility, and strength. In addition, it has good oxidation resistance and microstructure stability.[139] In 2018, Wei et al.[140] examined the impact of heat treatment on the mechanical properties and microstructure of the L-PBF-developed Ti–5Al–2.5Sn. As a consequence of the high cooling rate during the L-PBF process, the resultant microstructure included columnar prior-β grains with needles of martensitic α′ phase inside and a small portion of grain-boundary α stripes at the boundaries of the prior-β grains. More interestingly, the authors reported a superior combination of elongations and tensile strengths compared with a conventionally fabricated Ti–5Al–2.5Sn after the AM sample was heat treated at 650–850 °C for 2 h.

Ti–Al–Sn–Zr–Mo–Si is another near α alloy representing a pivotal choice among the high-temperature Ti-alloys. However, Nb and Ta can be added to further elevate the antioxidation efficiency at high temperatures by increasing the melting point. Zhou et al.[141] developed Ti–5.5Al–3.4Sn–3.0Zr–0.7Mo–0.3Si–0.4Nb–0.35Ta alloy in 2018 via the L-PBF method and compared it to the as-cast sample with identical chemical composition. The optimum process parameters were found to be 140 W laser power, a scanning speed of 400 mm s^{-1}, and a layer thickness of 0.08 mm. While the as-cast specimen exhibited a plate-like α phase, the as-built sample comprised acicular martensitic α′ phases. The oxidation behavior of both specimens was examined at 700 °C for 96 h. The AM sample, with a finer microstructure, exhibited a better high-temperature oxidation resistance; the mass gain of the as-built AM specimen was approximately 2.36 mg cm^{-2} for 96 h, which was less than that of the as-cast sample with 5.347 mg cm^{-2}. Moreover, the AM sample surface oxides were principally compact titanium oxide nanoparticles with a structure similar to a rod. In contrast, the surface oxides for the as-cast sample were titanium oxide nanoparticles with a rod-like structure and Al_2O_3 with a needle-like structure.

The high biocompatibility, low density, and superior corrosion behavior of CP-Ti have enabled the metal to be extensively applied in the aerospace, biomedical, and automotive industries.[142] However, the hexagonal close-packed structure of α-titanium contributes to anisotropic mechanical performance and poor deformability, leading to costly production and rugged product design in traditional fabrication methods.[143] In 2020, Pehlivan et al.[144] examined the influence of sample geometry and build direction on the mechanical properties of CP-Ti grade 2. **Figure 17** depicts the 3D microstructures for both deposition orientations (vertical and horizontal), with **Figure 18** showing a higher magnification of the sample microstructures. While the vertical and horizontal samples showed different microstructures, both contained columnar grains, as seen in Figure 18. However, the microstructure of the horizontal specimen exhibits thinner grains having widths below 200 μm and lengths surpassing 600 μm. In contrast, the vertical specimen contained relatively coarse columnar grains with widths of up to 200 μm and lengths up to 300 μm. The authors noticed that the samples with a cross-sectional area smaller than 1.5 mm^2 rely significantly on the build orientation, while the effect was considerably less noticeable in specimens with areas >1.5 mm^2. Moreover, mechanical properties and surface roughness were found to depend on the build orientation. Also, Mosallanejad et al.[51] investigated the influence of laser power and scan rate under constant energy densities on the microstructure and corrosion properties and reported laser power as being a more effective parameter; the sample produced with a lower laser power had a higher level of porosity and thinner alpha laths. According to the simulation results, this behavior was attributed to a larger melt pool formed at higher laser powers.

3.1.2. EBM

The average optimal mechanical properties of the as-built samples produced by the EBM method are summarized in **Figure 19**a using the literature data. The HIP and HT specimen properties are also included in Figure 19b for comparison. The figure illustrates that among the EBM alloys in their as-built state, the Ti55511 and Ti6242 alloys exhibit the highest UTS values. (Figure 19a), while the Ti6Al4V and Ti6242 alloys have the highest UTS values among the HT and HIPed samples (Figure 19b).

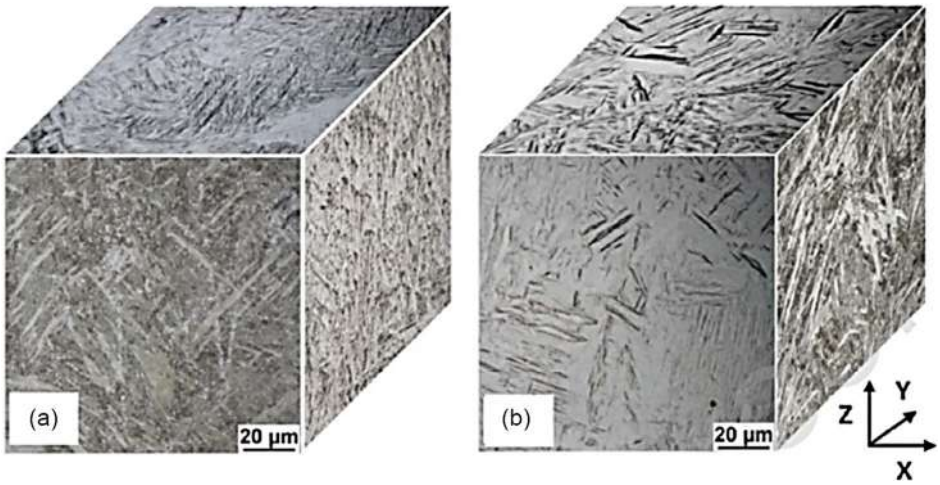

Figure 17. The 3D layout of microstructures displaying distinct: a) vertical build orientation and b) horizontal build orientation. Reproduced with permission.[144] Copyright 2020, Elsevier.

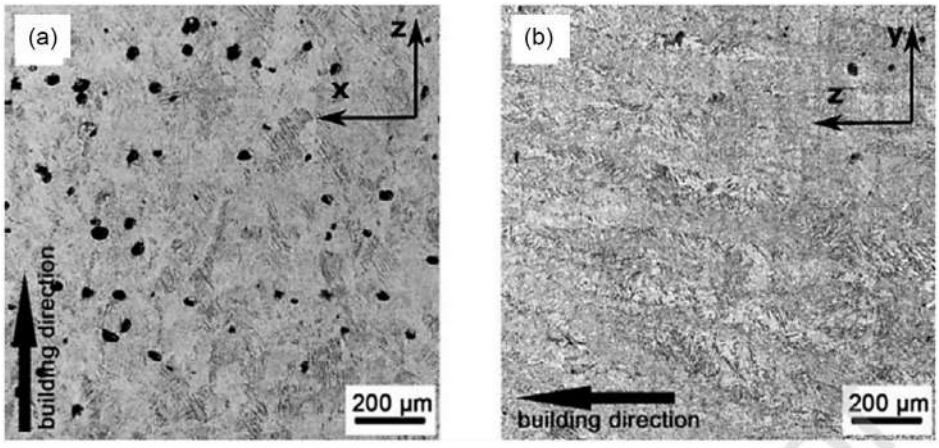

Figure 18. Specimens microstructure in two different directions: a) vertical and b) horizontal. Reproduced with permission.[144] Copyright 2020, Elsevier.

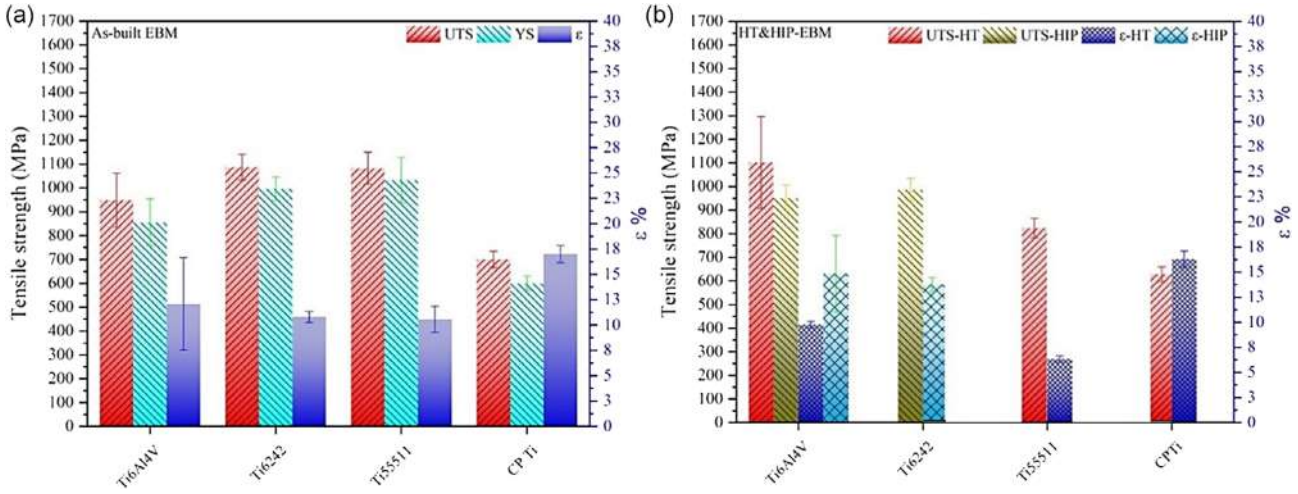

Figure 19. Average optimal tensile strength of alloy generated by EBM methods, a) as-built, b) HT, and HIP samples.

In 2019, Yang et al.[145] developed a Ti–24Nb–4Zr–8Sn rhombic dodecahedron and topology-optimized cell structure via EBM. They reported that at a specific strain cycle, the rhombic dodecahedron structure showed a higher recoverable strain than the optimized topology structure, citing the influence of stress distribution on struts. In addition, compared to the Ti–6Al–4V cellular structure, the cellular structure of the Ti–24Nb–4Zr–8Sn alloy with rhombic dodecahedron unit cell had a higher recovered strain. This behavior can be attributed to the superelasticity and superior strength-to-modulus ratio (σ/E) of the Ti–24Nb–4Zr–8Sn alloy. Furthermore, the recoverable strain of reticulated mesh was affected by cell shape, material properties of struts, and applied strain.

In 2020, Lopez et al.[146] investigated the effect of the HIP process on the mechanical properties of Ti–6Al–2Sn–4Zr–2Mo EBM fabricated via two different machines. The microstructure for the EBM-developed Ti6242 included equiaxed grains and consisted of acicular alpha-prime martensite having a width of ≈0.6 μm. These results were nearly identical for specimens generated by two different EBM machines, indicating similar thermal conditions for both machines. The as-built samples of Ti6242-experienced HIP postprocessing at 850, 950, and 1050 °C generated a mixture of acicular martensite and alpha at 850 °C, including blocky, refined grains. The optimized postprocess HIP temperature was 850 °C because it allowed the best mechanical properties with a yield strength of 0.9 GPa, a UTS of ≈1 GPa, and 15–16% elongation. In another work, Galati et al.[52] deeply investigated the processability of Ti6242 alloy. The authors utilized X-ray computed tomography (CT) analysis to evaluate the specimen density and defects and demonstrated that fully dense products could be manufactured by selecting a proper combination of process parameters for hatch and contour melting (**Figure 20**). The mechanical properties of the samples were reported to be comparable to as-cast Ti6242 alloy.

The Ti–6.5Al–3.5Mo–1.5Zr–0.3Si composition is a common $\alpha + \beta$ titanium alloy broadly utilized in the blades of aero-engines and compressor disks because of its excellent overall mechanical properties, including thermal stability at room and high

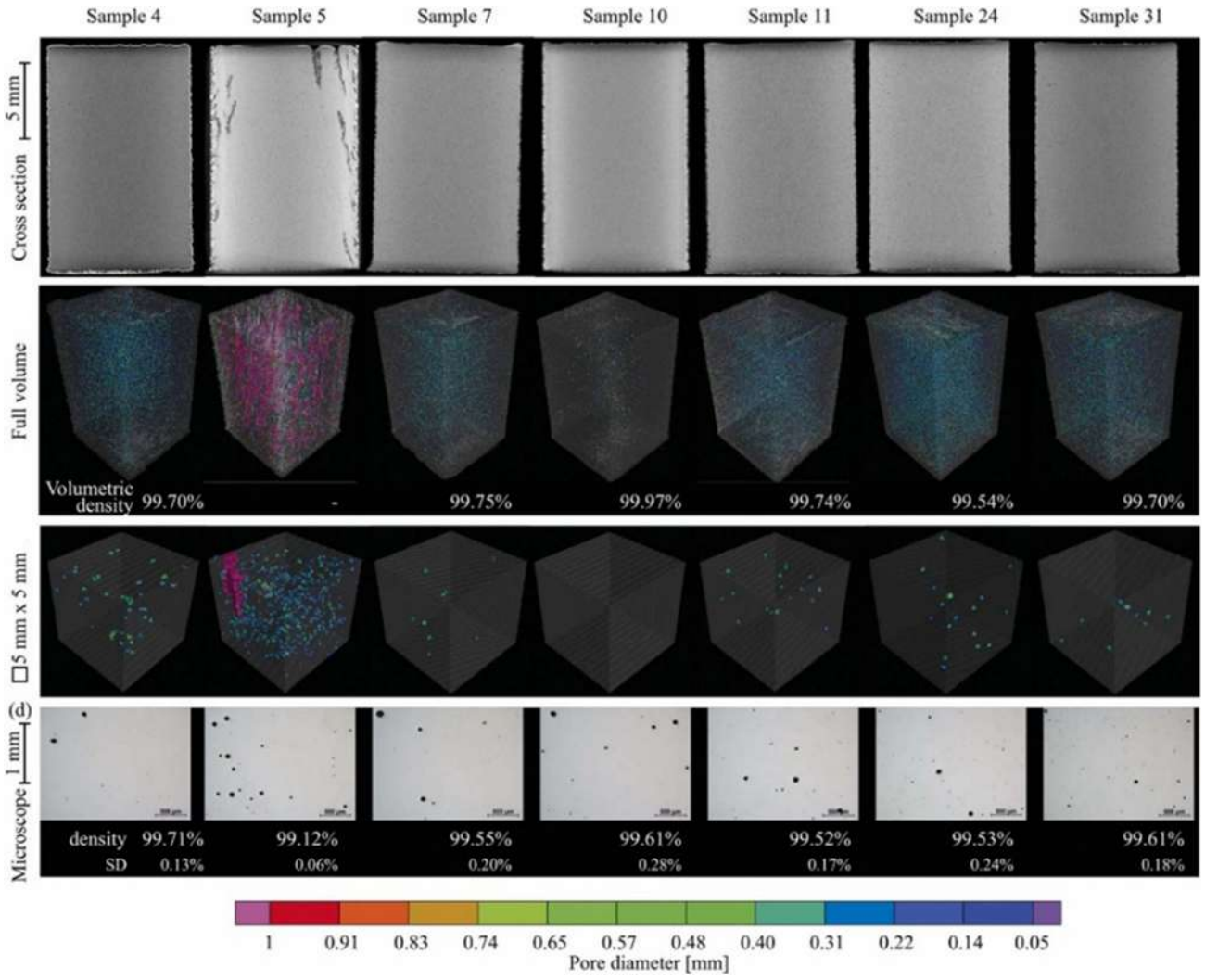

Figure 20. a) Cross-section, b) total volume porosity analysis, c) porosity distribution of the as-built Ti6242 samples obtained by X-Ray CT analysis, and d) light optical micrograph from the cross-section of the as-built samples. Reproduced with permission.[52] Copyright 2022, Elsevier.

temperatures, ductility, creep resistance, and strength.[147] Stepanova et al.[148] investigated the hydrogen impact on Ti–6.5Al–3.5Mo–1.5Zr–0.3Si specimens made via EBM by subjecting the samples to gas-phase hydrogenation at 650 °C. The results showed that hydrogenation could lead to the refinement of the alloy microstructure. Concurrently, due to δ-TiH hydride precipitation and redistribution of alloying elements, hydrogenation provoked the hardness enhancement in the alloy.

As a β stabilizing element, Nb is often added to Ti alloys to reduce the alloy elastic modulus. Several studies have shown that an Nb concentration of about 26% (at) is adequate for β-phase stabilization, achieving a low-modulus alloy. In contrast, concerning biocompatibility, Nb is recognized to be nontoxic.[149] In 2019, Khrapov et al.[150] manufactured Ti-26Nb via EBM. The fabricated alloy consisted of the Ti β phase. The increase in the energy input reduced the β-phase crystallite size and increased the lattice parameter. Also, the efficiency of Nb particle dissolution and alloy homogeneity was found to rely on the beam energy primarily. Despite this trend, crack-like voids were observed that were attributed to the poor flowability of the powder mixture, and insufficient local heating caused a weak bond between Ti α-phase and Nb particles.

Ti–36Nb–2Ta–3Zr–0.35O, commonly known as "gum metal" or TNTZO, is a beta-type titanium alloy renowned for its exceptional superelasticity, low elastic modulus, and excellent strength containing nontoxic elements. Accordingly, gum metal is a proper choice for biomedical purposes.[151] In 2015, Chen et al.[152] employed EBM to surface treatment Ti–36Nb–2Ta–3Zr–0.35O samples. The authors stated that the EBM technique was an efficient way to modify the surface, which remarkably modified the wear resistance and surface hardness of the TNTZO alloy. Low linear energy density and high scanning speed were identified as the two main reasons for decreasing the depth of the melting zone on the surface.

An outstanding combination of fracture toughness, creep resistance, and strength is offered by Ti–6Al–2.7Sn–4Zr–0.4Mo–0.45Si (TIMETAL 1100). The alloy's main commercial application is vehicle engine pipes. Adding 0.1%Y leads to the refinement of the TIMETAL 1100 microstructure and enhances its high-temperature features, stability, and ductility. Additionally, it changes the precipitation position of the titanium silicide from the α matrix to being constantly associated with the β phase. In 2015, Sheng-Lu et al.[153] investigated Ti–6Al–2.7Sn–4Zr–0.4Mo–0.45Si–0.1Y developed via EBM and compared the results with those of a forged-and-rolled sample. A fair and homogeneous dispersion of fine Y_2O_3 particles in a 50–250 nm size range was reported in the AMed sample matrix. In contrast, coarse and inhomogeneously distributed Y_2O_3 precipitates were noticed in the forged-and-rolled Ti600 sample, which also had cracked or debonded Y_2O_3 particles.

In 2017, Choi et al.[154] examined the mechanical features of CP-Ti and Ti6Al4V fabricated via EBM and compared them with those of the conventional CP-Ti and Ti6Al4V samples. Both CP-Ti and Ti6Al4V were built with the same parameters. However, the mechanical properties of the as-cast CP-Ti and the AMed CP-Ti developed by EBM were similar. In contrast, the mechanical properties of Ti6Al4V manufactured by EBM showed good mechanical properties but had lower fatigue limits, which could be linked to internal links.

In 2021, Del Guercio et al.[87] studied a novel strategy to assess the mechanical performance of Ti6Al4V lattice structures produced by the EBM. As shown in **Figure 21**, the authors produced three different unit cells and suggested that, apart from the cell size and typology, the structure's relative density is one of the principal factors that affect the lattice structure's mechanical behavior. Moreover, they observed that cell size and type had a negligible impact on the lattice microstructure. Also, the authors showed the absorbed energy up to failure to be closely correlated to the relative density.

3.1.3. DED

Laser-based DED technologies will be discussed first in this section, followed by works using WAAM. The average mechanical properties of the as-built samples by laser-based DED extracted from the literature are shown in **Figure 22**a. In addition, properties associated with the HT specimen are illustrated in Figure 22b. It should also be noted that in Figure 22a, the alloys developed by the laser-based DED technology without undergoing postprocessing steps had the highest UTS value. Furthermore, as shown in Figure 22b, the TA15 and TC11 alloys had the highest amount of UTS after heat treatment.

Molybdenum is observed to be nontoxic, allergy-free, and proper for controlling the body's pH. Furthermore, the addition of Mo to Ti improves corrosion resistance and biocompatibility. In 2019, Bhardwaj[110] investigated the corrosion and bioactivity of Ti–15Mo alloy. A schematic of the formation of partially unmelted Mo particles and the morphology of prior β grains

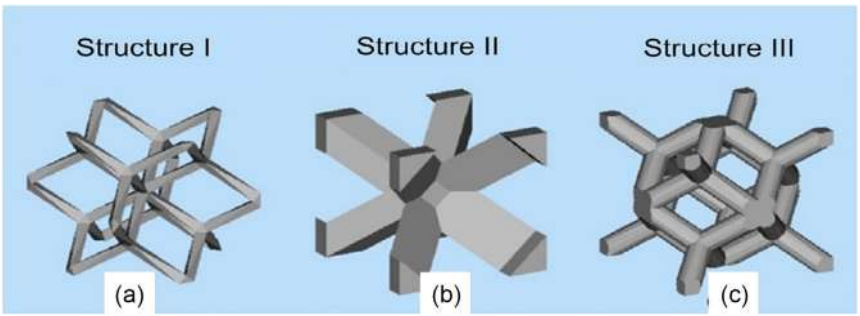

Figure 21. Three distinct structures: a) dode thin structure, b) G-structure, and c) rhombic dodecahedron structure. Reproduced with permission.[87] Copyright 2020, Springer Nature.

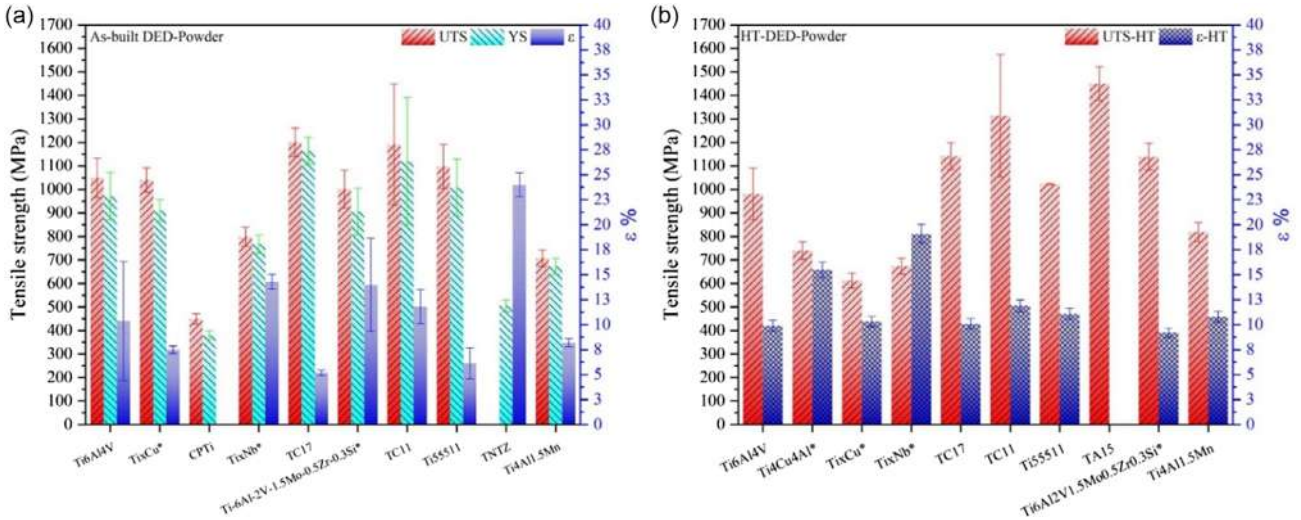

Figure 22. Average optimal tensile strength of alloy produced by laser-based DED methods: a) as-built, b) HT samples.

is presented in **Figure 23**.[155] Compared to vertical surfaces, the double oxide layer passivation created higher corrosion resistance on horizontal surfaces. Additionally, due to the low thermal gradients, the vertical specimens exhibited homogenous and more significant apatite formation due to higher surface topographic features and the type of surface morphology formed.

In 2018, Liu et al.[156] assessed the fatigue properties of the Ti–6.5Al–3.5Mo–l.5Zr–0.3Si alloy produced by laser-based DED. They reported that for the samples parallel to the deposition orientation, the fatigue limit was 365 MPa. In comparison, the value for the component perpendicular to the deposition orientation was 337 MPa, at a fatigue limit of 10^7 cycles and a stress ratio of 0.1 on a stress frequency of 20 and 40 Hz, respectively. Furthermore, the porosities were between 0.014% and 0.028%, with an average value of 0.02%. Thus, the column grain boundary formed throughout solidification was the proper place for initiating the fatigue cracks at the pores near the surface. The fatigue life of the specimen depended on the pore size and its distance from the surface.

In 2018, Wei et al.[157] evaluated the impact of heat treatment on the microstructure and mechanical properties of Ti–26Nb. The authors observed that heat treatment improved the ductility of the alloy but reduced its strength. In contrast, by raising the annealing temperature moderately, the strength of the alloy was seen to improve. The solution strengthening, owing to the unmelted Nb particles dissolution and the β grains coarsening, was identified as the possible factor creating variation trend of the mechanical features with annealing temperature. Hence, the authors reported that a suitable equilibrium of ductility and strength could be achieved via an annealing process at 850 °C for 30 min.

In 2016, Li et al.[158] developed Ti–6Al–2V–1.5Mo–0.5Zr–0.3Si, a low-cost modern α + β titanium composition, by adding various alloying elements to Ti6Al4V using the laser-based DED method. They reported that the as-built specimen consisted of a basket-weave microstructure with a more delicate lamellar α phase than the Ti6Al4V alloy. The microstructure feature was linked to the typical thermal cycles during the AM process. Compared to the Ti6Al4V, microhardness was improved by adding Zr, Mo, and Si due to solid-solution hardening effects. The microhardness could be enhanced further by a finer basket-weave structure. Additionally, the Ti–6Al–2V–1.5Mo–0.5Zr–0.3Si alloy exhibited a better tensile strength than Ti6Al4V.

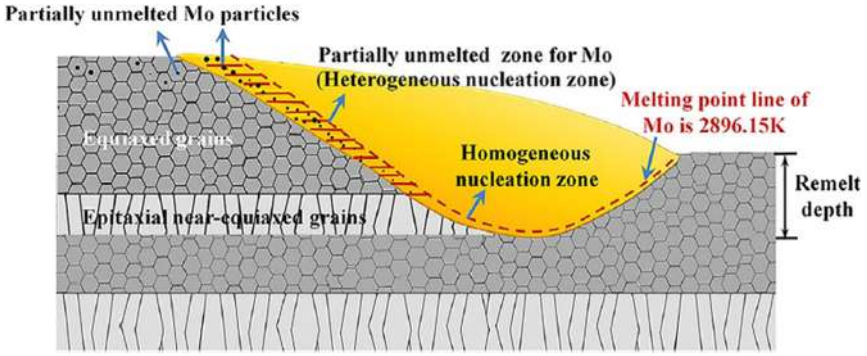

Figure 23. Schematic showing the formation of unmelted Mo particles and the morphology of prior β grains. Reproduced with permission.[155] Copyright 2019, John Wiley and Sons Inc.

In 2020, Mantri et al.[159] investigated the laser engineering Net Shaping (LENS) of Ti–4Cu and Ti–4Cu–4Al, which is conventionally challenging to cast due to the impact of β-flaking. The results showed that homogeneous, segregation-free compositions could be obtained due to the LENS's high cooling rates. Heat treatments were conducted, and there was no retained β even with the highest cooling rate in the water-quenched specimen. Furthermore, the presence of the α and Ti_2Cu phases at the appropriate length scale led to a suitable compound of ductility and strength in all heat treatment situations. Moreover, high strengths were noted in the water-quenched specimens for both the binary and ternary alloys.

In 2019, Wang et al.[160] investigated the production of Ti–55 511 alloy by the DED method. The authors reported that factors such as α_p laths, continuous α_{GB}, lack of fusion, and voids might affect crack propagation in the DED Ti–55 511 alloy under periodic loads. Under these circumstances, the impact of primary α_p laths was the most significant because it provided the coalescence of microcracks and the propagation of secondary cracks.

In 2019, Chen et al.[161] investigated the effect of deformation on a DED-fabricated Ti–6.5Al–1Mo–1V–2Zr alloy microstructure and α texture after a high strain rate. Increasing the temperature from 930 to 970 °C declined the component flow stress throughout deformation to 2% at a strain rate of $3000 \pm 100\,s^{-1}$. Subsequent annealing at 970 °C improved uniform ductility by 14.3% more than that obtained at 950 °C. In 2018, the spatial distribution of the α phase in the DED Ti–10V–2Fe–3Al alloy was studied by Jiao et al.[162] They observed that the α phase precipitates uniformly in grain, with three types of morphologies. Eventually, the model of α phase spatial distribution described the formation of various microstructure morphologies, reducing the crystallographic grain orientation.

In 2019, Saboori et al.[163] examined the influence of nozzle position on the melt pool geometry during the laser-based DED of Ti6Al4V. The authors stated that the lateral nozzle location was a highly influential factor, besides other parameters like laser and feeding parameters, in determining the final melt pool shape and the number of defects. Moreover, it was noted that the heat input and powder capture efficiency could change by adjusting the distance between the powder nozzle and substrate. The optimal length between the substrate and the nozzle should be investigated to achieve defect-free deposition. Finally, it was suggested that even when employing an uneven powder, the formation of a melt pool with a proper shape was still feasible at the ideal nozzle distance.

The optimal mechanical characteristics of the WAAM method for as-built samples are shown in **Figure 24**a. Furthermore, the resultant properties of the HT specimen are also illustrated in Figure 24b. It can be noticed that the highest UTS in as-built samples belongs to the TC11 and Ti6Al4V alloys, whereas the highest UTS after HT treatment belongs to the Ti8V3Al6Cr4Mo4Zr alloy among the analyzed data.

In 2019, Lu et al.[40] employed HWAAM to produce Ti–6.5Al–2Zr–1Mo–1 V alloy and employed X-ray CT to study the samples. The porosity in the melt pool overlap zone was 1.56 to 1.63 times lower than that in the pool body zone. The fusion border had the most pores, with the melt pool overlap containing less porosity than the pool body. Pore equivalent diameters were mainly in a narrow range. Hydrogen rejection caused spherical gas pores. Wire warpage, arc length variation, and high heat generated irregular fusion pores.

In 2020, Bermingham et al.[164] used WAAM to produce Ti–3Al–8V–6Cr–4Mo–4Zr samples and examined the influence of postbuild heat treatments. Primarily, β-phase led to high ductility and average strength in solution-treated Ti–3Al–8V–6Cr–4Mo–4Zr (reported to excel Ti6Al4V). Furthermore, α precipitates made from duplex aging increased the strength and hardness of the sample depending on aging time and temperature. Compared with additively manufactured α + β Ti6Al4V, Ti–3Al–8V–6Cr–4Mo–4Zr was shown to offer excellent ductility or strength thanks to its ability to be intensely hardened by aging and postbuild solution heat treatment.

In 2020, Zhang et al.[165] manufactured Ti–5Al–2Sn–2Zr–4Mo–4Cr via wire feed electron beam AM. They observed rough

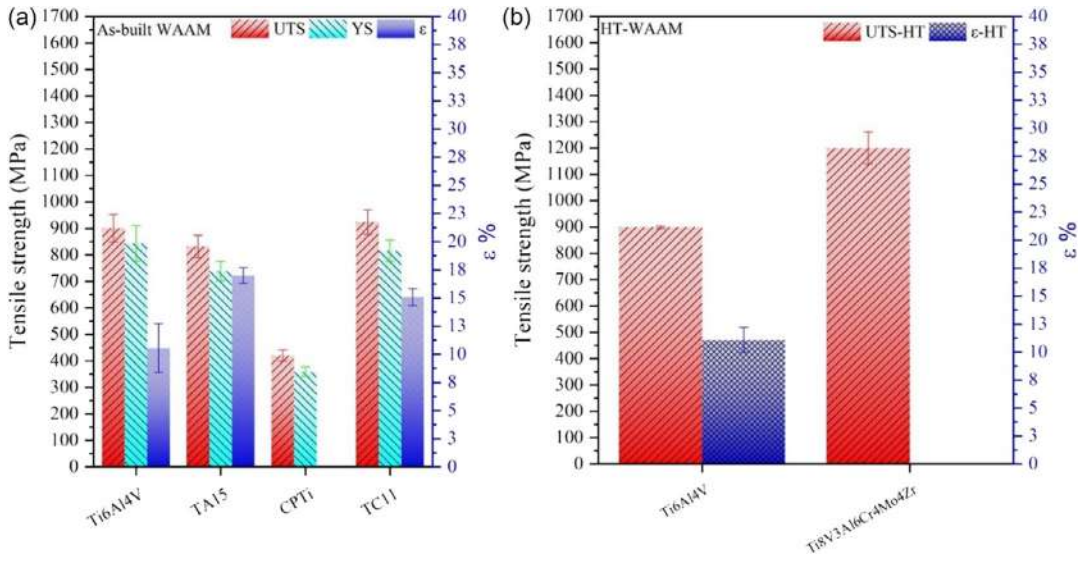

Figure 24. Average optimal tensile strength of alloy generated by WAAM methods: a) as-built and b) HT samples.

columnar grains that grow epitaxially from the substrate in the as-built microstructure. The mechanical properties and microstructure of the EBAMed near β Ti–5Al–2Sn–2Zr–4Mo–4Cr correlated quantitatively (**Figure 25**). Continuous cracks also promoted intergranular cracks in specimens aging at low or high temperatures.

In 2018, Li et al.[166] implemented the TC11 to create four thin-walled specimens via HWAAM, and the mechanical features and microstructure were analyzed. The work included reducing the thermal gradient (G) by increasing the layer thickness and tailoring the entire columnar morphology into equiaxed and short columnar grains.

TA15, a near-α Ti alloy, has been extensively employed in aircraft and engines as an applicable structural titanium alloy with good damage endurance. According to the service conditions, evaluating the deformed manner and mechanical attributes of the TA15 alloy under high strain rates is vital. In 2021, Xue et al.[167] developed a thin-walled structure using the WAAM method using TA15 wires, where 0.1 wt% boron element was added to tailor the resultant microstructure along with the stable phases. The addition of trace B element, besides the thermal situation governing the WAAM process, led to the formation of equiaxed prior-β grains in the as-built specimens, as noticed in **Figure 26**.

Another work added a trace amount of B to Ti6Al4V[168] during the WAAM process. The effect of boron on the solidification behavior of the resultant liquid is schematically illustrated in **Figure 27**, where it can be observed that the higher freezing range of the boron solute raises the mushy zone and contributes to curved columnar grains. The lateral growth is limited by the lateral rejection of boron-rich solute from the sides and base of columnar dendrites, which presents an occasion for neighboring dendrites to grow. Ultimately, the authors reported that adding trace boron did not remarkably affect strength while enhancing ductility in the as-built condition. However, boron was found to promote strength and ductility by 10% and 40%, respectively, following heat treatment compared to the unmodified Ti6Al4V alloy.

3.2. Indirect Methods

In 2020, Tang et al.[169] developed Ti6Al4V via BJT. The capillary infiltration of the polymer binder is schematically shown in **Figure 28**. First, according to Figure 28a, the binder droplets are selectively deposited on the powder bed when discharged from the nozzle. Then, the droplet is forced to keep flowing on the powder surface by the initial kinetic energy, as shown in Figure 28b. Next, the binder solution is actively inserted into the powder because of the capillary force in the porous bed, as depicted in Figure 28c. Finally, following the heating of the powder bed, the polymer binder is cross-linked when the water in the solution is evaporated. The self-crosslinking polymer binder serves as a connecting bridge between the particles, facilitating the bonding of powder particles, as illustrated in Figure 28d.

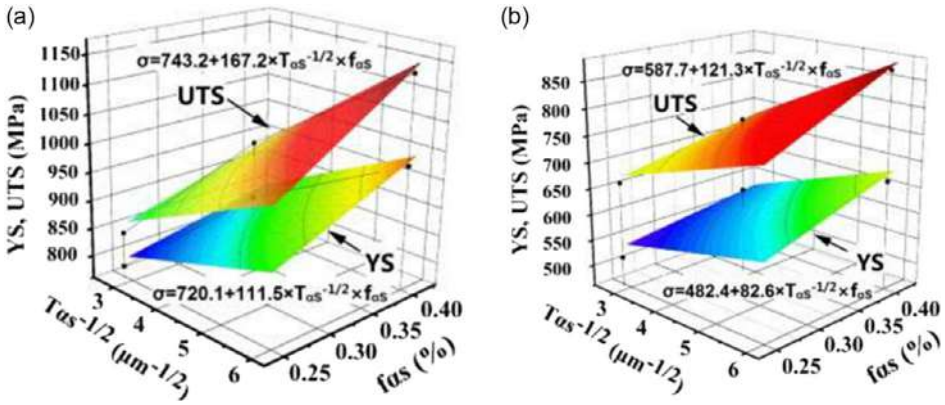

Figure 25. The change in the tensile strength with microstructural features α_S ($f_{\alpha S}$), volume fraction, and inverse of the α_S thickness square root ($T_{\alpha S}^{-1/2}$) at room temperature a) and 400 °C b). Reproduced with permission.[165] Copyright 2020, Elsevier.

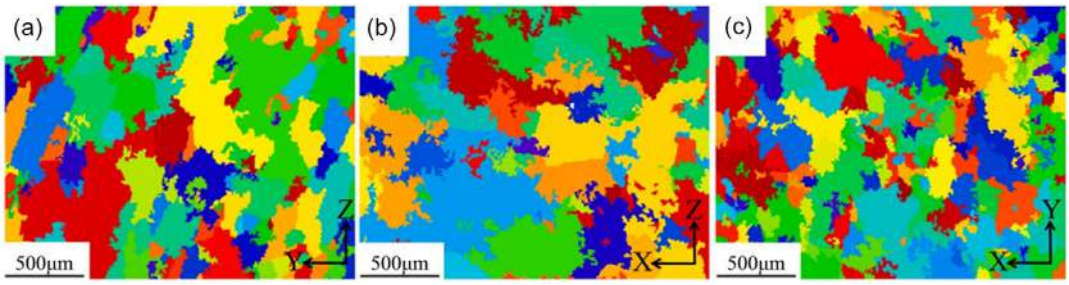

Figure 26. The reconstructed electron backscatter diffraction (EBSD) map of prior-β phase a–c) of the as-deposited sample in YOZ (a), XOZ (b), and XOY (c) planes. Reproduced with permission.[167] Copyright 2021, Elsevier.

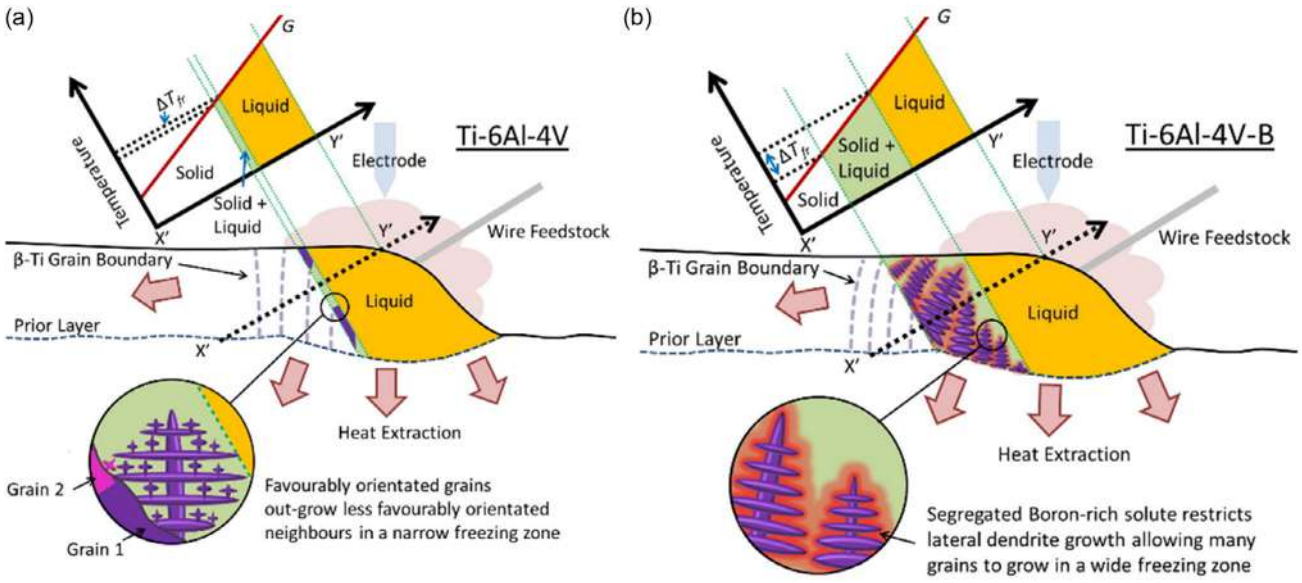

Figure 27. Side view schematic explaining how the boron solute induces an extensive freezing range; a) boron-free Ti6Al4V and b) Ti6Al4V modified with trace boron additions. Reproduced with permission.[168] Copyright 2015, Elsevier.

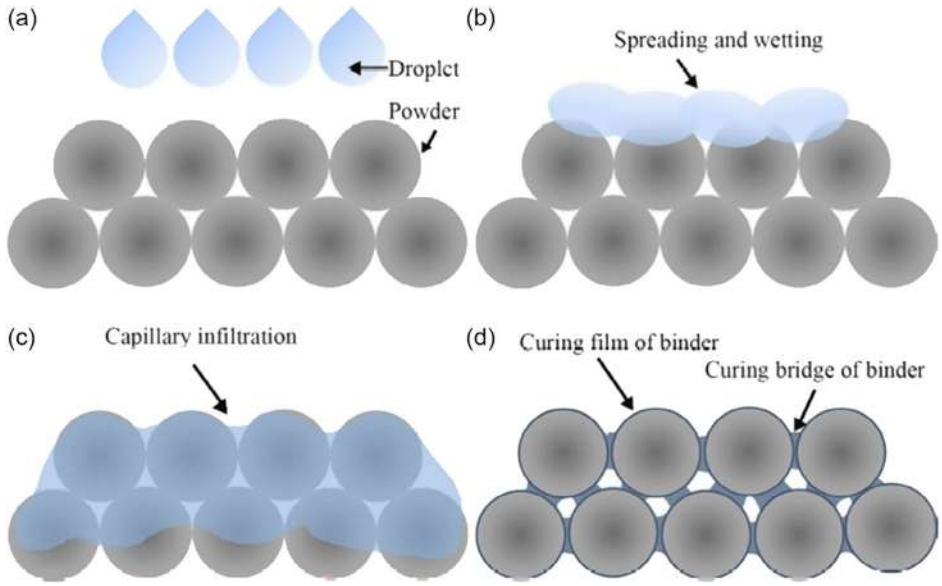

Figure 28. Capillary infiltration principle based on polymer binder, a) droplets deposited selectively, b) spread of binder solution, c) solution penetrates the powder layer, and d) after heating, the curing film and bridge are developed. Reproduced under the terms of the CC BY license.[169] Copyright 2020, MDPI.

Tang et al.[169] investigated the influence of fine powders. As a result, capillary force improved from 8.35 to 16.27 kPa, increasing compression strength from 1.5 to 3.21 MPa. BJT was also utilized by Polozov et al.[170] to study the AM feasibility of Ti2AlNb alloy using Nb, Ti, and Al, accompanied by reactive sintering and annealing. The results demonstrated that Ti–22Al–25Nb porous components with the microstructure of ($B2 + Ti_2AlNb$) could be fabricated by employing the proposed procedure.

Yadav et al.[171] conducted a feasibility study on the fabrication of TiAl samples via the BJT method. The method included BTJ of Ti–6Al–4V followed by Al being introduced via pressureless ex situ infiltration. The authors reported dense parts exhibiting a Young modulus of 145 GPa, a compressive strength of 1.4 GPa, and a bending strength of 483 MPa.

4. Future Perspective

AM offers an array of advantages in terms of cost-effective approaches for a broad range of direct and indirect procedures,

such as quick production, the ability to manufacture a wide variety of components with complicated geometry, increased proficiency, fine grain size and phase composition, and decreased energy consumption. The distinct thermal and processing characteristics of additive manufacturing methods offer opportunities for developing novel titanium alloys with microstructures and characteristics unattainable by traditional methods. Advancements in AM methods have yielded substantial benefits in several critical sectors, including aerospace, aviation, and biomedical applications, as illustrated in **Figure 29**. AM has provided the aerospace industry with the capability to prototype new products featuring lightweight designs and toolless production rapidly.

Furthermore, complicated organs can be produced by AM techniques. The ability of AM to allow for product customization and timely dispatch is an emerging trend in AM. Direct and indirect AM methods propose an encouraging perspective for producing novel Ti alloys of unique compositions, microstructures, and characteristics. Nonetheless, similar to welding, AM of titanium is considered a significant challenge due to the nonequilibrium features of AM processes and the complicated influence of process parameters on microstructure and subsequent mechanical properties. The metallurgical properties accountable for microstructural and mechanical characteristics should provide a robust analytical foundation for future AM studies.

Direct and indirect processes contribute to a novel procedure for manufacturing designed materials with distinctive characteristics. As a result, AM has grown to compete with conventional production methods regarding expense, production rate, safety, and precision, making it a next-generation technology, as considered by many specialists.

Furthermore, the use of prealloyed powders as powder feedstock has some limitations, including a narrow range of composition, high costs, and limited availability. To address the issue of inflexibility in powder-based additive manufacturing, an elemental powder mixture can be used.[54] This approach shows promise in developing new titanium alloy compositions for powder-based AM, which could offer advantages in terms of cost and speed. However, it is important to note that this method presents challenges related to inhomogeneity and segregation during the in situ alloying process in AM.

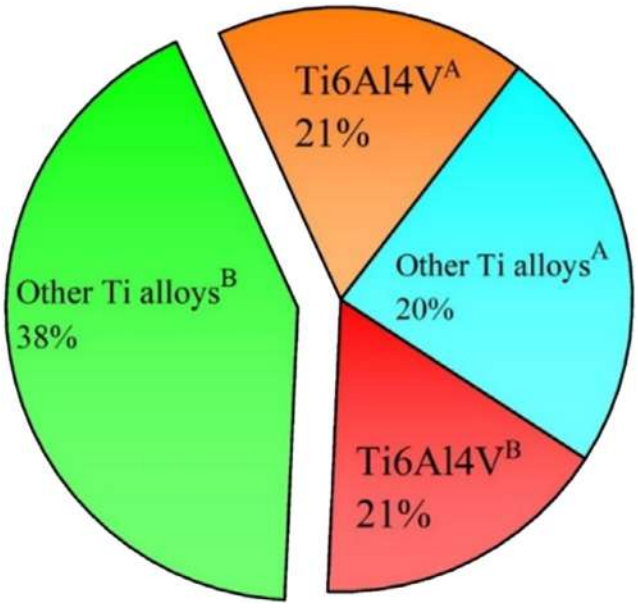

Figure 29. Typical breakdown of AM titanium alloys application, A denotes aerospace and aviation application and B stands for biomedical application.

5. Industrial Applications

AM is a collection of manufacturing technologies deemed essential to fulfill the distinctive demands of the industry. Being a critical technology that has become the principal product innovation and advancement element in this imminent industrial revolution, the force within advancements of AM metal science, made by accelerated prototyping for engineering goals, is swiftly evolving and shifting, approaching the generation of parts with great value composed of superior materials. In addition, utilization cases tend to include critical products such as aviation and biomedical tools.

From a metallurgical perspective, alloy compositions with minor deviations from the eutectic composition have traditionally been favored for alloy design. This results in hierarchical structures that display distinctive length scales, including primary dendrites embedded within a finely layered eutectic matrix. The configuration of these characteristics depends on the solidification conditions during growth. As the growth velocity or cooling rate increases, their particle sizes generally decrease. This allows for substantial size-hardening effects and paves the way for material design through rapid solidification technique. Although this particular category of Ti-based eutectic alloys has been studied for years, there is no economically and technically feasible processing method for producing large samples or actual components; consequently, the proposed alloys are rarely suitable for use in industry. Laser-based AM, specifically L-PBF, offers intrinsically rapid solidification and cooling rates; therefore, it could serve as a viable strategy for addressing the issue mentioned above.[172]

The possibility of modifying the traditional designs and saving considerable expense and energy is manifested by using complicated cooling channels in heat exchangers with high-performance applications and coatings with wear-resistant behavior in refinery and petrochemical industries.[173,174]

5.1. Biomedical

The biomedical business has been influenced mainly by AM since it can efficiently offer the customizations required in the industry. Personalized patient models are in three-dimensional sections acquired through customized software. One example is the use of dental implants and custom-fit crowns, which have disrupted traditional fabrication methods for dental tools, bridges, and partial frames. The advantages of AM are the accelerated production of customizing gadgets to generate 3D patterns of implants for use in the human body.

While the porous components benefit bone build-up, implementing flat and pore-free parts with reasonable accuracy is also obligatory for medical purposes.[175] Most metal implants were previously manufactured via traditional routes; however, using

those traditional methods, lattice structure-based implants are challenging to make. Lattice structures, like orthopedic implants, are crucial because their porous design allows adjacent bone tissue to adhere and proliferate. Triply periodic minimum surface lattice structures with larger surface area to volume ratios have linked design that facilitates nutrition and waste transportation.[22] As mentioned earlier, AM has been a promising approach to meeting these demands.

Also, materials contributing to adequate durability and biocompatibility are now utilized in medical tools, such as Co, Cr, and Ti compositions, which AM already manufactures.[175]

Titanium alloys have a strong presence in the biomedical field, particularly for implants. The study highlights newly developed titanium alloys like Ti2448 and Ti5553, showcasing their potential for biomedical applications. Biomedical companies can consider these alloys for manufacturing implants with improved biocompatibility. **Figure 30** represents some AM-built Ti6Al4V biomedical implants manufactured by the EBM method.[176]

5.2. Aerospace

In aerospace, the AM parts are often meant to perform at severe temperatures and pressures. The possible reduction in manufacturing times and costs presents an excellent motive for assessing AM technology. Aerospace purposes dictate stringent policies and standards for methods and segments. Notable savings may be obtained by decreasing the number of authenticated components and methods, like joints, creating a segment. Reducing the final weight leads to meaningful savings in different areas, like diminishing fuel consumption conservation throughout regular commercial flights. At the same time, the reduction of waste by producing valuable materials such as Ti or Ni-based compositions is crucial in attesting AM applicability. A comprehensive lifespan analysis, which compares the expenses of each approach and the entire production chain from beginning to end, has revealed significant cost savings, primarily due to reduced weight like titanium versus steel in lightweight design.[177] Other hypothetical applications can also be considered for the aerospace sector. AM capability to create complex geometries enables the production of aerospace components with optimized designs. This is particularly valuable for components like brackets, airfoils, and engine parts, where specific designs are intended to enhance aerodynamics and fuel efficiency. **Figure 31** comparatively shows an aerospace Ti-bracket produced by conventional and AM methods, and **Figure 32** shows a potential aerospace application. The research delves into the mechanical properties of titanium alloys processed through AM methods. This knowledge allows aerospace engineers to understand the material characteristics better and tailor designs for optimal performance and safety.

5.3. Automotive

The apparent tendency of the automotive sector toward using AM metal processing parts resides in the accelerated prototyping

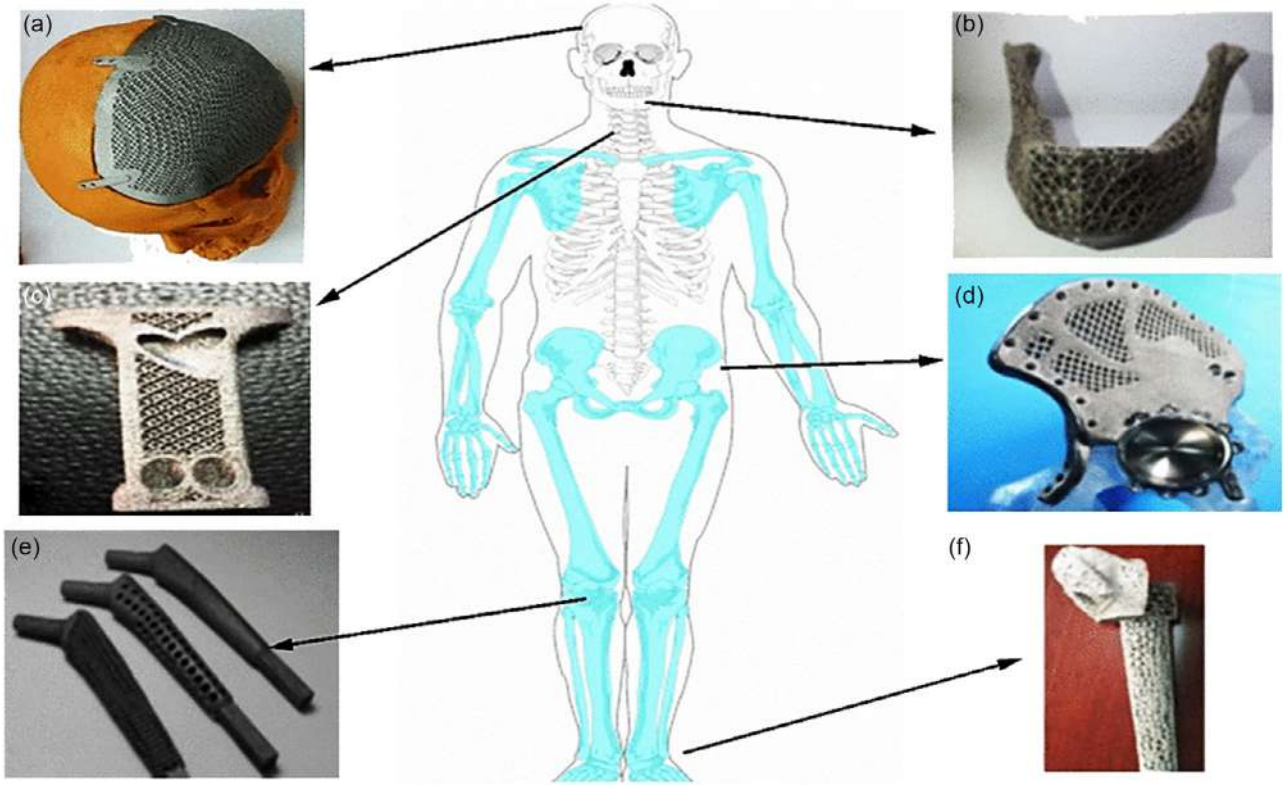

Figure 30. EBM developed Ti6Al4V implants: a) cranial plate, b) mandibular prosthesis, c) cervical vertebral fusion cage, d) pelvic implant, e) hip stems, and f) ankle prosthetics human skeleton. Reproduced with permission.[176] Copyright 2021, Elsevier.

Figure 31. Ti cabin bracket Airbus A350 XWB produced by a) conventional and b) additive manufacturing methods. Reproduced with permission.[178] Copyright 2023, Elsevier.

of practical components and reduced energy consumption from utilizing AM-built components. The production of one-of-a-kind and rare parts, like the ones used in classic automotive mending, is sought occasionally. Although mass production of automobile parts is beyond the capabilities of current metal AM technologies, AM procedures based on a CAD model of a metal component to produce a sand mold or plastic pattern are gaining traction. Cost is a secondary consideration in racing car design, while reducing weight and creative design freedom take precedence. The implementation of AMed titanium components in the automotive industry with the aim of lightweight holds immense potential for fuel economy. It has been estimated that fuel economy can be improved by approximately 6% to 8% per 10 kg reduction in weight. This can lead to improved fuel efficiency and reduced emissions, which aligns with the industry sustainability goals. The above goals provide a proving ground for AM technologies in the automobile sector.[178] The flexibility of AM in producing customized parts enables automotive manufacturers to craft unique designs and features that align with consumer preferences. In terms of large-scale production, this study suggests that DED is an appropriate method for

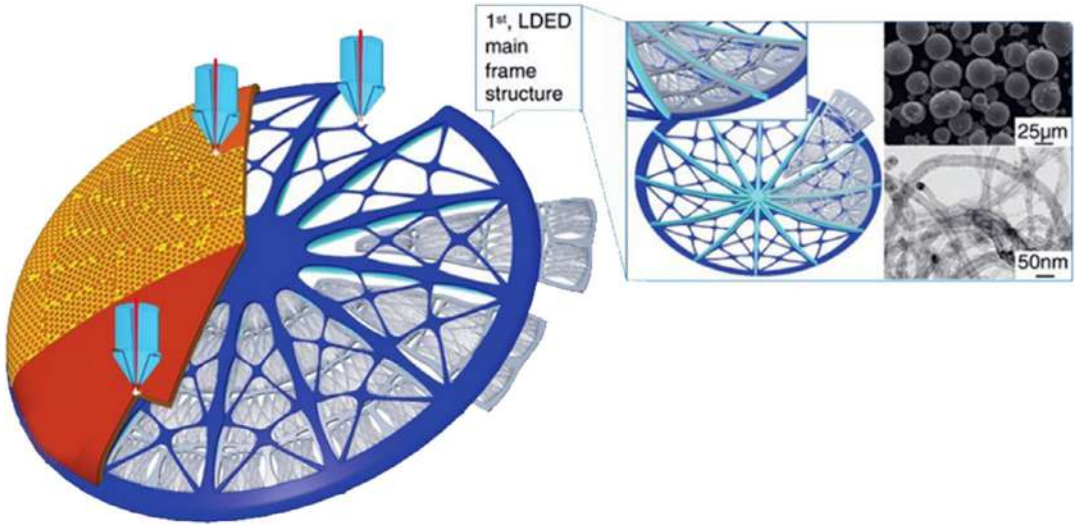

Figure 32. An aerospace component with the potential for additive manufacturing production The main frame structure can be a carbon nanotube (CNT) reinforced Ti-based composite. Reproduced with permission.[179] Copyright 2021, The American Association for the Advancement of Science.

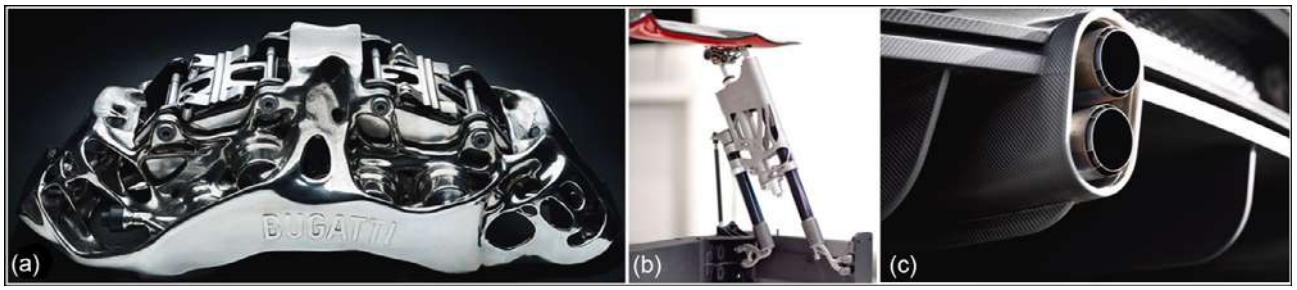

Figure 33. a) An eight-piston monobloc brake caliper, b) an active spoiler bracket, and c) tailpipe trim covers. Reproduced with permission.[180] Copyright 2023, Elsevier.

automotive companies to manufacture large structural and engine components. **Figure 33** shows multiple examples of Bugatti AMed titanium parts in different car applications.

6. Conclusion

AM is emerging into a formidable future production process. The flexibility and resilience of printing technologies are significant and positive benefits of 3D printing over traditional production processes. The inter-relationship between the Ti alloy composition and the AM technique was discussed in this review. While AM technologies present significant difficulties in producing flawless, isotropic, and homogenous metallic components, their nonequilibrium nature makes it possible to develop unique microstructures, phase constituents, and composition designs. Despite current constraints, including slow printing rates and topological concerns with printed components, the ability of AM to produce complex structures is a distinct advantage.

Furthermore, notable development has been established in the AM of titanium alloys. It allows the fabrication of Ti components despite the challenges encountered by conventional processes. This review assesses a wide range of emerging fabrication methods proper for producing titanium alloy parts. The review examines direct and indirect approaches like L-PBF, EBM, and DED for direct methods and BJT and ADAM for indirect techniques. This research exhibits more promise for manufacturing larger-scale components via DED, which can become more widely adopted to manufacture aerospace structures.

In contrast, other methods are more suitable for generating complex geometries and delicate parts for biomedical and aviation purposes. A large anisotropy is usually observed among titanium alloys regarding mechanical properties. Besides, post-processing techniques have a fundamental and decisive role in improving tensile strength. The stress relief heat treatment, especially for L-PBF, modifies the specimen phase composition and influences the bar's tensile properties. The principal merit of EBM is the electron beam energy, which can scan the surface at a remarkably tremendous rate and allows for preheating. This results in a novel melting procedure, which not only leads to the reduction of the anisotropy but can produce parts with lower levels of defects. Also, due to the stress-relief annealing, the residual stresses of EBM components are significantly lower compared to L-PBF parts. Hence, EBM is principally accommodated for alloys that are challenging or impracticable to produce. Numerous Ti-based alloys were investigated and provided to researchers throughout this text to maximize the benefits of additive manufacturing. This research not only provides a comprehensive understanding of titanium alloy processing through AM methods but also offers actionable insights for industries. These insights can guide decision-making in material selection, component design, and production processes, ultimately leading to more sustainable, efficient, and innovative solutions in the aerospace, biomedical, and automotive sectors. The findings bridge the gap between traditional manufacturing methods and the transformative potential of AM, empowering industries to harness the benefits of this cutting-edge technology.

Conflict of Interest

The authors declare no conflict of interest.

Keywords

mechanical properties, metal additive manufacturing, microstructure, processability, titanium alloys

Received: July 22, 2023
Revised: October 20, 2023
Published online: November 10, 2023

[1] M. Dadkhah, J.-M. Tulliani, A. Saboori, L. Iuliano, *J. Eur. Ceram. Soc.* **2023**, *43*, 6635.
[2] A. Behjat, M. Shamanian, F. Sadeghi, L. Iuliano, A. Saboori, *Mater. Lett.* **2023**, *355*, 135363.
[3] S. Huang, S. L. Sing, G. de Looze, R. Wilson, W. Y. Yeong, *J. Mech. Behav. Biomed. Mater.* **2020**, *108*, 103775.
[4] R. Ghanavati, E. Lannunziata, E. Norouzi, S. Bagherifard, L. Iuliano, A. Saboori, *Mater. Lett.* **2023**, *349*, 134793.
[5] V. Viale, J. Stavridis, A. Salmi, F. Bondioli, A. Saboori, *Int. J. Adv. Manuf. Technol.* **2022**, *123*, 2159.
[6] X. J. Tian, S. Q. Zhang, A. Li, H. M. Wang, *Mater. Sci. Eng., A* **2010**, *527*, 1821.
[7] C. Sun, Y. Wang, M. D. McMurtrey, N. D. Jerred, F. Liou, J. Li, *Appl. Energy* **2021**, *282*, 116041.
[8] T. Barbin, D. V. Velôso, L. Del Rio Silva, G. A. Borges, A. G. C. Presotto, V. A. R. Barão, M. F. Mesquita, *J. Mech. Behav. Biomed. Mater.* **2020**, *108*, 103821.
[9] M. R. Bandekhoda, M. H. Mosallanejad, M. Atapour, L. Iuliano, A. Saboori, *Met. Mater. Int.* **2023**, https://doi.org/10.1007/s12540-023-01496-6.
[10] V. Juechter, M. M. Franke, T. Merenda, A. Stich, C. Körner, R. F. Singer, *Addit. Manuf.* **2018**, *22*, 118.
[11] N. Schehl, V. Kramb, J. Dierken, J. Aldrin, E. Schwalbach, R. John, *AIP Conf. Proc.* **2018**, *1949*, 20008.
[12] F. H. Sam. Froes, M. N. Gungor, M. Ashraf Imam, *JOM* **2007**, *59*, 28.
[13] A. Vance, K. Bari, A. Arjunan, *Biomed. Phys. Eng. Express* **2019**, *5*, 35008.
[14] A. Barbas, A.-S. Bonnet, P. Lipinski, R. Pesci, G. Dubois, *J. Mech. Behav. Biomed. Mater.* **2012**, *9*, 34.
[15] D. Eylon, F. H. Froes, R. W. Gardiner, *JOM* **1983**, *35*, 35.
[16] A. Arjunan, A. Baroutaji, A. Latif, *Results Eng.* **2021**, *11*, 100252.
[17] S. Sun, M. Brandt, M. S. Dargusch, *Int. J. Mach. Tools Manuf.* **2010**, *50*, 663.
[18] R. K. Gupta, V. A. Kumar, C. Mathew, G. S. Rao, *Mater. Sci. Eng., A* **2016**, *662*, 537.
[19] A. V. S. R. Prasad, K. Ramji, G. L. Datta, *Procedia Mater. Sci.* **2014**, *5*, 2567.
[20] GE Agrees to Purchase Controlling Shares of Arcam AB, GE Addit **2019**, https://www.geadditive.com (accessed: January 2023).
[21] M. Mehrpouya, A. Vosooghnia, A. Dehghanghadikolaei, B. Fotovvati, *Handbooks in Advanced Manufacturing*, Elsevier **2021**.
[22] T.-S. Jang, D. Kim, G. Han, C.-B. Yoon, H.-D. Jung, *Biomed. Eng. Lett.* **2020**, *10*, 505.
[23] P. Moghimian, T. Poirié, M. Habibnejad-Korayem, J. A. Zavala, J. Kroeger, F. Marion, F. Larouche, *Addit. Manuf.* **2021**, *43*, 102017.
[24] G. Del Guercio, M. Galati, A. Saboori, P. Fino, L. Iuliano, *Acta Metall. Sin.* **2020**, *33*, 183.

[25] A. Saboori, A. Abdi, S. A. Fatemi, G. Marchese, S. Biamino, H. Mirzadeh, *Mater. Sci. Eng., A* **2020**, *792*, 139822.
[26] H. Lu, W. Deng, K. Luo, Y. Chen, J. Wang, J. Lu, *Addit. Manuf.* **2023**, *63*, 103416.
[27] L. Bhandari, V. Gaur, *Addit. Manuf.* **2022**, *60*, 103227.
[28] C. De Formanoir, S. Michotte, O. Rigo, L. Germain, S. Godet, *Mater. Sci. Eng., A* **2016**, *652*, 105.
[29] A. Poudel, M. Salman Yasin, S. Shao, N. Shamsaei, in *Solid Freeform Fabrication Symp.*, University of Texas at Austin **2022**, pp. 1895–1903.
[30] A. Goulas, D. Southcott-Engstrøm, R. J. Friel, R. A. Harris, in *Solid Freeform Fabrication 2016: Proc. 26th Annual Int. Solid Freeform Fabrication Symp. – An Additive Manufacturing Conf. Reviewed Paper*, University of Texas at Austin **2016**, pp. 2271–2281.
[31] T. P. Moran, P. E. Carrion, S. Lee, N. Shamsaei, N. Phan, D. H. Warner, *Materials* **2022**, *15*, 2051.
[32] A. Soltani-Tehrani, J. P. Isaac, H. V. Tippur, D. F. Silva, S. Shao, N. Shamsaei, *Int. J. Fatigue* **2023**, *167*, 107343.
[33] A. Arjunan, M. Demetriou, A. Baroutaji, C. Wang, *J. Mech. Behav. Biomed. Mater.* **2020**, *102*, 103517.
[34] H. D. Nguyen, A. Pramanik, A. K. Basak, Y. Dong, C. Prakash, S. Debnath, S. Shankar, I. S. Jawahir, S. Dixit, D. Buddhi, *J. Mater. Res. Technol.* **2022**, *18*, 4641.
[35] H.-J. Yi, J.-W. Kim, Y.-L. Kim, S. Shin, *Met. Mater. Int.* **2020**, *26*, 1235.
[36] M. Pellizzari, A. Jam, M. Tschon, M. Fini, C. Lora, M. Benedetti, *Materials* **2020**, *13*, 2792.
[37] Y. J. Liu, S. J. Li, H. L. Wang, W. T. Hou, Y. L. Hao, R. Yang, T. B. Sercombe, L. C. Zhang, *Acta Mater.* **2016**, *113*, 56.
[38] H. Schwab, F. Palm, U. Kühn, J. Eckert, *Mater. Des.* **2016**, *105*, 75.
[39] H. D. Carlton, K. D. Klein, J. W. Elmer, *Sci. Technol. Weld. Joining* **2019**, *24*, 465.
[40] T. Lu, C. Liu, Z. Li, Q. Wu, J. Wang, T. Xu, J. Liu, H. Wang, S. Ma, *J. Alloys Compd.* **2020**, *817*, 153334.
[41] H. Bai, H. Deng, L. Chen, X. Liu, X. Qin, D. Zhang, T. Liu, X. Cui, *Metals* **2021**, *11*, 534.
[42] J. Ran, X. Sun, S. Wei, Z. Chen, H. Zhao, *Crystals* **2021**, *11*, 495.
[43] V. Hoppe, A. Pawlak, P. Szymczyk-Ziółkowska, T. Jaśkiewicz, M. Rusińska, B. Dybała, *Mater. Des.* **2022**, *217*, 110546.
[44] M. Hein, N. F. Lopes Dias, S. Pramanik, D. Stangier, K.-P. Hoyer, W. Tillmann, M. Schaper, *Materials* **2022**, *15*, 3774.
[45] N. Hafeez, S. Liu, E. Lu, L. Wang, R. Liu, L.C. Zhang, *J. Alloys Compd.* **2019**, *790*, 117.
[46] M. S. Dargusch, G. Wang, D. Kent, M. Bermingham, J. Venezuela, J. E. Frith, Z. Yu, S. Yu, Z. Shi, *ACS Biomater. Sci. Eng.* **2019**, *5*, 5844.
[47] S. Pilz, T. Gustmann, F. Günther, M. Zimmermann, U. Kühn, A. Gebert, *Mater. Des.* **2022**, *216*, 110516.
[48] I. Polozov, V. Sufiiarov, A. Popovich, D. Masaylo, A. Grigoriev, *J. Alloys Compd.* **2018**, *763*, 436.
[49] A. Jam, A. du Plessis, C. Lora, S. Raghavendra, M. Pellizzari, M. Benedetti, *Addit. Manuf.* **2022**, *50*, 102556.
[50] H. R. Ghorbani, M. H. Mosallanejad, M. Atapour, M. Galati, A. Saboori, *J. Mater. Res. Technol.* **2022**, *20*, 180.
[51] M. H. Mosallanejad, S. Sanaei, M. Atapour, B. Niroumand, L. Iuliano, A. Saboori, *Acta Metall. Sin.* **2022**, *35*, 1453.
[52] M. Galati, S. Defanti, A. Saboori, G. Rizza, E. Tognoli, N. Vincenzi, A. Gatto, L. Iuliano, *Addit. Manuf.* **2022**, *50*, 102564.
[53] A. Saboori, D. Gallo, S. Biamino, P. Fino, M. Lombardi, *Appl. Sci.* **2017**, *7*, 883.
[54] M. H. Mosallanejad, B. Niroumand, A. Aversa, A. Saboori, *J. Alloys Compd.* **2021**, *872*, 159567.
[55] W. Frazier, P. C. Llc, E. Marquard, *ASM Handbook*, ASM International, Materials Park, OH **2021**.
[56] A. Aversa, A. Saboori, G. Marchese, L. Iuliano, M. Lombardi, P. Fino, *J. Mater. Eng. Perform.* **2021**, *30*, 8689.
[57] Y. Hu, W. Cong, *Ceram. Int.* **2018**, *44*, 20599.
[58] D.-S. Shim, G.-Y. Baek, J.-S. Seo, G. Y. Shin, K. P. Kim, K. Y. Lee, *Opt. Laser Technol.* **2016**, *86*, 69.
[59] R. Barros, F. J. G. Silva, R. M. Gouveia, A. Saboori, G. Marchese, S. Biamino, A. Salmi, E. Atzeni, *Metals* **2019**, *9*, 1290.
[60] L.-C. Zhang, H. Attar, *Adv. Eng. Mater.* **2016**, *18*, 463.
[61] M. R. Jandaghi, A. Saboori, L. Iuliano, M. Pavese, *Mater. Sci. Eng., A* **2021**, *828*, 142109.
[62] J. J. Beaman, D. L. Bourell, C. C. Seepersad, D. Kovar, *J. Manuf. Sci. Eng.* **2020**, *142*, 110812.
[63] M. Aristizabal, P. Jamshidi, A. Saboori, S. C. Cox, M. M. Attallah, *Mater. Lett.* **2020**, *259*, 126897.
[64] S. Vock, B. Klöden, A. Kirchner, T. Weißgärber, B. Kieback, *Prog. Addit. Manuf.* **2019**, *4*, 383.
[65] S. Chowdhury, N. Yadaiah, C. Prakash, S. Ramakrishna, S. Dixit, L. R. Gupta, D. Buddhi, *J. Mater. Res. Technol.* **2022**, *20*, 2109.
[66] L. E. Murr, S. M. Gaytan, D. A. Ramirez, E. Martinez, J. Hernandez, K. N. Amato, P. W. Shindo, F. R. Medina, R. B. Wicker, *J. Mater. Sci. Technol.* **2012**, *28*, 1.
[67] Z. Fu, C. Körner, *Eur. J. Mater.* **2022**, *2*, 54.
[68] B. Dutta, *Encyclopedia of Materials: Metals and Alloys*, Elsevier, Amsterdam/New York **2022**, pp. 66–84.
[69] A. Saboori, A. Aversa, G. Marchese, S. Biamino, M. Lombardi, P. Fino, *Appl. Sci.* **2019**, *9*, 3316.
[70] N. Shamsaei, A. Yadollahi, L. Bian, S. M. Thompson, *Addit. Manuf.* **2015**, *8*, 12.
[71] D. G. Ahn, *Int. J. Precis. Eng. Manuf.-Green Technol.* **2021**, *8*, 703.
[72] S. Hossein Nedjad, M. Yildiz, A. Saboori, *Sci. Technol. Weld. Joining* **2023**, *28*, 1.
[73] S. Dahat, K. Hurtig, J. Andersson, A. Scotti, *J. Manuf. Mater. Process.* **2020**, *4*, 14.
[74] T. A. Rodrigues, V. Duarte, R. M. Miranda, T. G. Santos, J. P. Oliveira, *Materials* **2019**, *12*, 1121.
[75] S. M. Gaytan, M. A. Cadena, H. Karim, D. Delfin, Y. Lin, D. Espalin, E. MacDonald, R. B. Wicker, *Ceram. Int.* **2015**, *41*, 6610.
[76] I. Campbell, T. Wohlers, *Markforged: Taking a Different Approach to Metal Additive Manufacturing*, Inovar Communications Ltd **2017**.
[77] M. Galati, P. Minetola, *Materials* **2019**, *12*, 4122.
[78] M. Roccetti Campagnoli, M. Galati, A. Saboori, *J. Manuf. Processes* **2021**, *72*, 320.
[79] A. Dehghan-Manshadi, M. J. Bermingham, M. S. Dargusch, D. H. StJohn, M. Qian, *Powder Technol.* **2017**, *319*, 289.
[80] F. A. Shah, M. Trobos, P. Thomsen, A. Palmquist, *Mater. Sci. Eng., C* **2016**, *62*, 960.
[81] A. Azarniya, X. G. Colera, M. J. Mirzaali, S. Sovizi, F. Bartolomeu, M. K. St Weglowski, W. W. Wits, C. Y. Yap, J. Ahn, G. Miranda, F. S. Silva, H. R. M. Hosseini, S. Ramakrishna, A. A. Zadpoor, *J. Alloys Compd.* **2019**, *804*, 163.
[82] W. Xu, M. Brandt, S. Sun, J. Elambasseril, Q. Liu, K. Latham, K. Xia, M. Qian, *Acta Mater.* **2015**, *85*, 74.
[83] O. M. Mcgee, S. Geraghty, C. Hughes, P. Jamshidi, D. P. Kenny, M. M. Attallah, C. Lally, *J. Mech. Behav. Biomed. Mater.* **2022**, *134*, 105388.
[84] M. Bisht, N. Ray, F. Verbist, S. Coeck, *Addit. Manuf.* **2018**, *22*, 302.
[85] A. Mohammadhosseini, D. Fraser, S. H. Masood, M. Jahedi, *Mater. Res. Innovations* **2013**, *17*, s106.
[86] N. Hrabe, R. Kircher, T. Quinn, in *23rd Annual Int. Solid Freeform Fabrication Symp. - An Additive Manufacturing Conf. SFF 2012*, University of Texas at Austin **2012**, pp. 1045–1058.
[87] G. Del Guercio, M. Galati, A. Saboori, *Met. Mater. Int.* **2021**, *27*, 55.
[88] M. Asherloo, Z. Wu, M. H. Delpazir, E. Ghebreiesus, S. Fryzlewicz, R. Jiang, B. Gould, M. Heim, D. Nelson, M. Marucci, M. Paliwal, A. D. Rollett, A. Mostafaei, *Addit. Manuf.* **2022**, *56*, 102875.

[89] M. Khorasani, A. Ghasemi, U. S. Awan, E. Hadavi, M. Leary, M. Brandt, G. Littlefair, W. O'Neil, I. Gibson, *Int. J. Adv. Manuf. Technol.* **2020**, *111*, 2891.
[90] M. Yakout, M. A. Elbestawi, S. C. Veldhuis, *J. Manuf. Processes* **2020**, *52*, 181.
[91] B. Zhou, J. Zhou, H. Li, F. Lin, *Mater. Sci. Eng., A* **2018**, *724*, 1.
[92] L. Thijs, F. Verhaeghe, T. Craeghs, J. V. Humbeeck, J.-P. Kruth, *Acta Mater.* **2010**, *58*, 3303.
[93] J. Han, M. Wu, W. Duan, *Materials* **2020**, *13*, 937.
[94] M. A. Galindo-Fernández, K. Mumtaz, P. E. J. Rivera-Díaz-del-Castillo, E. I. Galindo-Nava, H. Ghadbeigi, *Mater. Des.* **2018**, *160*, 350.
[95] M. Simonelli, N. T. Aboulkhair, P. Cohen, J. W. Murray, A. T. Clare, C. Tuck, R. J. M. Hague, *Mater. Charact.* **2018**, *143*, 118.
[96] B. Wysocki, P. Maj, R. Sitek, J. Buhagiar, K. Kurzydłowski, W. Święszkowski, *Appl. Sci.* **2017**, *7*, 657.
[97] P. Gao, W. Huang, H. Yang, G. Jing, Q. Liu, G. Wang, Z. Wang, X. Zeng, *J. Mater. Sci. Technol.* **2020**, *39*, 144.
[98] L. Zhou, T. Yuan, R. Li, J. Tang, M. Wang, F. Mei, *J. Alloys Compd.* **2018**, *762*, 289.
[99] N. Kang, X. Lin, C. Coddet, X. Wen, W. Huang, *Mater. Lett.* **2020**, *267*, 127544.
[100] J. Guzmán, R. M. Nobre, E. R. Nunes, D. L. Bayerlein, R. B. Falcão, E. Sallica-Leva, J. B. F. Neto, H. R. Oliveira, V. L. Chastinet, F. J. G. Landgraf, *J. Mater. Res. Technol.* **2021**, *10*, 1372.
[101] C. Qiu, Ni. J. E. Adkins, M. M. Attallah, *Mater. Sci. Eng. A* **2013**, *578*, 230.
[102] N. Hafeez, J. Liu, L. Wang, D. Wei, Y. Tang, W. Lu, L. C. Zhang, *Addit. Manuf.* **2020**, *34*, 101264.
[103] C. Schulze, M. Weinmann, C. Schweigel, O. Keßler, R. Bader, *Materials* **2018**, *11*, 124.
[104] J. C. Wang, Y. J. Liu, P. Qin, S. X. Liang, T. B. Sercombe, L. C. Zhang, *Mater. Sci. Eng., A* **2019**, *760*, 214.
[105] J. Wang, Y. Liu, C. D. Rabadia, S.-X. Liang, T. B. Sercombe, L.-C. Zhang, *J. Mater. Sci. Technol.* **2021**, *61*, 221.
[106] R. Ummethala, P. S. Karamched, S. Rathinavelu, N. Singh, A. Aggarwal, K. Sun, E. Ivanov, L. Kollo, I. Okulov, J. Eckert, K. G. Prashanth, *Materialia* **2020**, *14*, 100941.
[107] F. Haftlang, A. Zarei-Hanzaki, H. R. Abedi, J. Málek, E. Farabi, H. Beladi, *Met. Mater. Int.* **2020**, *26*, 467.
[108] Y. H. Zhou, W. P. Li, L. Zhang, S. Y. Zhou, X. Jia, D. W. Wang, M. Yan, *J. Mater. Process. Technol.* **2020**, *276*, 116398.
[109] T. Ishimoto, K. Hagihara, K. Hisamoto, S.-H. Sun, T. Nakano, *Scr. Mater.* **2017**, *132*, 34.
[110] T. Bhardwaj, M. Shukla, N. K. Prasad, C. P. Paul, K. S. Bindra, *Met. Mater. Int.* **2020**, *26*, 1015.
[111] M. Simonelli, Y. Y. Tse, C. Tuck, *Mater. Sci. Eng., A* **2014**, *616*, 1.
[112] G. Kasperovich, J. Hausmann, *J. Mater. Process. Technol.* **2015**, *220*, 202.
[113] L. Zhou, T. Yuan, R. Li, J. Tang, M. Wang, L. Li, C. Chen, *J. Alloys Compd.* **2019**, *775*, 1164.
[114] L. C. Zhang, T. B. Sercombe, *Key Eng. Mater.* **2012**, *520*, 226.
[115] J. P. Luo, Y. J. Huang, J. Y. Xu, J. F. Sun, M. S. Dargusch, C. H. Hou, L. Ren, R. Z. Wang, T. Ebel, M. Yan, *Mater. Sci. Eng., C* **2020**, *114*, 110903.
[116] S. L. Sing, W. Y. Yeong, F. E. Wiria, *J. Alloys Compd.* **2016**, *660*, 461.
[117] E. Chlebus, B. Kuźnicka, T. Kurzynowski, B. Dybała, *Mater. Charact.* **2011**, *62*, 488.
[118] Y. J. Liu, Y. S. Zhang, L. C. Zhang, *Materialia* **2019**, *6*, 100299.
[119] T. W. Xu, S. S. Zhang, F. S. Zhang, H. C. Kou, J. S. Li, *Mater. Sci. Eng., A* **2016**, *654*, 249.
[120] P. Qin, Y. Liu, T. B. Sercombe, Y. Li, C. Zhang, C. Cao, H. Sun, L.-C. Zhang, *ACS Biomater. Sci. Eng.* **2018**, *4*, 2633.
[121] M. H. Mosallanejad, B. Niroumand, A. Aversa, D. Manfredi, A. Saboori, *J. Alloys Compd.* **2021**, *857*, 157558.
[122] B. He, J. Li, X. Cheng, H.-M. Wang, *Mater. Sci. Eng., A* **2017**, *699*, 229.
[123] T. Maimaitiyili, K. Mosur, T. Kurzynowski, N. Casati, H. Van Swygenhoven, *Materials* **2020**, *13*, 1723.
[124] A. Chamanfar, T. Pasang, A. Ventura, W. Z. Misiolek, *Mater. Sci. Eng., A* **2016**, *663*, 213.
[125] R. Gaddam, B. Sefer, R. Pederson, M.-L. Antti, *IOP Conf. Ser.: Mater. Sci. Eng.* **2013**, *48*, 12002.
[126] H. Fan, S. Yang, *Mater. Sci. Eng., A* **2020**, *788*, 139533.
[127] S. Sui, Y. Chew, Z. Hao, F. Weng, C. Tan, Z. Du, G. Bi, *Adv. Powder Mater.* **2022**, *1*, 100002.
[128] Z. Zhu, F. L. Ng, H. L. Seet, S. M. L. Nai, *J. Alloys Compd.* **2022**, *895*, 162648.
[129] H. C. Kaushik, M. H. Korayem, A. Hadadzadeh, *Mater. Sci. Eng., A* **2022**, *860*, 144294.
[130] C. Iantaffi, C. L. A. Leung, Y. Chen, S. Guan, R. C. Atwood, J. Lertthanasarn, M. S. Pham, M. Meisnar, T. Rohr, P. D. Lee, *Addit. Manuf. Lett.* **2021**, *1*, 100022.
[131] Y. Chen, S. J. Clark, L. Sinclair, C. L. A. Leung, S. Marussi, T. Connolley, R. C. Atwood, G. J. Baxter, M. A. Jones, I. Todd, P. D. Lee, *Addit. Manuf.* **2021**, *41*, 101969.
[132] A. Kreitcberg, V. Brailovski, S. Prokoshkin, *J. Mater. Process. Technol.* **2018**, *252*, 821.
[133] E. Alabort, D. Barba, A. De Diego, M. V. Aguirre-Cebrian, R. C. Reed, in *A Novel Titanium Alloy for Additively Manufactured Orthopaedic Implants BT - TMS 2020 149th Annual Meeting & Exhibition Supplemental Proc.*, Springer International Publishing, Cham **2020**, pp. 267–276.
[134] V. V. Joshi, C. Lavender, V. Moxon, V. Duz, E. Nyberg, K. S. Weil, *J. Mater. Eng. Perform.* **2013**, *22*, 995.
[135] H. Azizi, H. Zurob, B. Bose, S. R. Ghiaasiaan, X. Wang, S. Coulson, V. Duz, A. B. Phillion, *Addit. Manuf.* **2018**, *21*, 529.
[136] X. Q. Jiang, X. G. Fan, M. Zhan, R. Wang, Y. F. Liang, *Mater. Des.* **2021**, *203*, 109589.
[137] Q. J. Sun, X. Xie, *Mater. Sci. Eng., A* **2018**, *724*, 493.
[138] C. Cai, X. Wu, W. Liu, W. Zhu, H. Chen, J. C. D. Qiu, C. N. Sun, J. Liu, Q. Wei, Y. Shi, *J. Mater. Sci. Technol.* **2020**, *57*, 51.
[139] A. Iltaf, F. N. Khan, T. Shehbaz, M. Junaid, *Proc. Inst. Mech. Eng., Part L* **2021**, *235*, 1952.
[140] K. Wei, Z. Wang, X. Zeng, *Mater. Sci. Eng., A* **2018**, *709*, 301.
[141] Y. Zhou, S. F. Wen, B. Song, X. Zhou, Q. Teng, Q. S. Wei, Y. S. Shi, *Mater. Des.* **2016**, *89*, 1199.
[142] X. P. Li, J. Van Humbeeck, J. P. Kruth, *Mater. Des.* **2017**, *116*, 352.
[143] R. K. Quinn, N. R. Armstrong, *J. Electrochem. Soc.* **1978**, *125*, 1790.
[144] E. Pehlivan, M. Roudnicka, J. Dzugan, M. Koukolikova, V. Králík, M. Seifi, J. J. Lewandowski, D. Dalibor, M. Daniel, *Addit. Manuf.* **2020**, *35*, 101403.
[145] H. X. Yang, S. J. Li, W. T. Hou, Y. L. Hao, R. Yang, R. D. K. Misra, *Mater. Technol.* **2020**, *35*, 881.
[146] M. Lopez, C. Pickett, E. Arrieta, L. E. Murr, R. B. Wicker, M. Ahlfors, D. Godfrey, F. Medina, *Materials* **2020**, *13*, 2604.
[147] D. Banerjee, J. C. Williams, *Acta Mater.* **2013**, *61*, 844.
[148] E. Stepanova, N. Pushilina, M. Syrtanov, R. Laptev, E. Kashkarov, *Int. J. Hydrogen Energy* **2019**, *44*, 29380.
[149] M. A. Surmeneva, A. Koptyug, D. Khrapov, Y. F. Ivanov, T. Mishurova, S. Evsevleev, O. Prymak, K. Loza, M. Epple, G. Bruno, R. A. Surmenev, *J. Mater. Process. Technol.* **2020**, *282*, 116646.
[150] D. Khrapov, M. Surmeneva, A. Koptioug, R. Surmenev, *J. Phys. Conf. Ser.* **2019**, *1347*, 12126.
[151] M. Besse, P. Castany, T. Gloriant, *Acta Mater.* **2011**, *59*, 5982.
[152] Z. Chen, Y. Liu, H. Wu, W. Zhang, W. Guo, H. Tang, N. Liu, *Appl. Surf. Sci.* **2015**, *357*, 2347.

[153] S.-L. Lu, H.-P. Tang, M. Qian, Q. Hong, L.-Y. Zeng, D. H. Stjohn, *J. Cent. South Univ.* **2015**, *22*, 2857.
[154] Y. S. Choi, C. L. Kim, G. H. Kim, B. S. Lee, C. W. Lee, D. G. Lee, *Appl. Mech. Mater.* **2017**, *873*, 54.
[155] H. Tan, T. Hu, F. Zhang, Y. Qiu, A. T. Clare, *Adv. Eng. Mater.* **2019**, *21*, 1900152.
[156] Z. Liu, P. Liu, L. Wang, Y. Lu, X. Lu, Z. X. Qin, H. M. Wang, *Mater. Sci. Eng., A* **2018**, *716*, 140.
[157] J. Wei, H. Sun, D. Zhang, L. Gong, J. Lin, C. Wen, *Materials* **2019**, *12*, 61.
[158] G.-C. Li, J. Li, X.-J. Tian, X. Cheng, B. He, H. M. Wang, *Mater. Sci. Eng., A* **2017**, *684*, 233.
[159] S. A. Mantri, T. Alam, Y. Zheng, J. C. Williams, R. Banerjee, *Addit. Manuf.* **2020**, *32*, 101067.
[160] K. Wang, R. Bao, T. Zhang, B. Liu, Z. Yang, B. Jiang, *Int. J. Fatigue* **2019**, *124*, 217.
[161] R. Chen, C. Tan, Z. You, Z. Li, S. Zhang, Z. Nie, X. Yu, X. Zhao, *Mater. Sci. Eng., A* **2019**, *750*, 81.
[162] Z. Jiao, J. Fu, Z. Li, X. Cheng, H. Tang, H. Wang, *Mater. Des.* **2018**, *154*, 108.
[163] A. Saboori, S. Biamino, M. Lombardi, S. Tusacciu, M. Busatto, M. Lai, P. Fino, *Powder Metall.* **2019**, *62*, 213.
[164] M. J. Bermingham, D. Kent, B. Pace, J. M. Cairney, M. S. Dargusch, *Mater. Sci. Eng., A* **2020**, *791*, 139646.
[165] G. Zhang, H. Xiong, H. Yu, R. Qin, W. Liu, H. Yuan, *Mater. Des.* **2020**, *195*, 109063.
[166] Z. Li, C. Liu, T. Xu, L. Ji, D. Wang, J. Lu, S. Ma, H. Fan, *Mater. Sci. Eng., A* **2019**, *742*, 287.
[167] L. Xue, J. Xiao, Z. Nie, F. Hao, R. Chen, C. Liu, X. Yu, C. Tan, *Mater. Sci. Eng., A* **2021**, *800*, 140310.
[168] M. J. Bermingham, D. Kent, H. Zhan, D. H. Stjohn, M. S. Dargusch, *Acta Mater.* **2015**, *91*, 289.
[169] S. Aksenov, V. Mikolaenko, *Metals* **2020**, *10*, 1353.
[170] I. Polozov, V. Sufiiarov, A. Shamshurin, *Mater. Lett.* **2019**, *243*, 88.
[171] P. Yadav, Z. Fu, M. Knorr, N. Travitzky, *Adv. Eng. Mater.* **2020**, *22*, 3.
[172] J. Gussone, K. Bugelnig, P. Barriobero-Vila, J. C. Da Silva, U. Hecht, C. Dresbach, F. Sket, P. Cloetens, A. Stark, N. Schell, J. Haubrich, G. Requena, *Appl. Mater. Today* **2020**, *20*, 100767.
[173] M. Schmidt, M. Merklein, D. Bourell, D. Dimitrov, T. Hausotte, K. Wegener, L. Overmeyer, F. Vollertsen, G. N. Levy, *CIRP Ann.* **2017**, *66*, 561.
[174] U. M. Dilberoglu, B. Gharehpapagh, U. Yaman, M. Dolen, *Procedia Manuf.* **2017**, *11*, 545.
[175] T. D. Ngo, A. Kashani, G. Imbalzano, K. T. Nguyen, D. Hui, *Composites, Part B* **2018**, *143*, 172.
[176] J. A. Tamayo, M. Riascos, C. A. Vargas, L. M. Baena, *Heliyon* **2021**, *7*, e06892.
[177] A. A. Shapiro, J. P. Borgonia, Q. N. Chen, R. P. Dillon, B. Mcenerney, R. Polit-Casillas, L. Soloway, *J. Spacecr. Rockets* **2016**, *53*, 952.
[178] R. Leal, F. M. Barreiros, L. Alves, F. Romeiro, J. C. Vasco, M. Santos, C. Marto, *Int. J. Adv. Manuf. Technol.* **2017**, *92*, 1671.
[179] D. Gu, X. Shi, R. Poprawe, D. L. Bourell, R. Setchi, J. Zhu, *Science* **2021**, *372*, eabg1487.
[180] P. Nyamekye, S. Rahimpour Golroudbary, H. Piili, P. Luukka, A. Kraslawski, *Adv. Ind. Manuf. Eng.* **2023**, *6*, 100112.

Mohammadhossein Mosallanejad is currently a post-doctoral research associate at the Department of Management and Production Engineering, Politecnico di Torino, and a member of the Integrated Additive Manufacturing Center at the same institution. Through his primary research focus on additive manufacturing of metallic components, he has authored several experimental and review papers on various aspects of AM, including process-structure properties and the development of novel alloys.

Ata Abdi got his M.Sc. in materials science and engineering from Khaje Nasir University. He is a materials researcher specializing in metallurgy, focusing on the intricate challenges of metal additive manufacturing. He has authored published five papers in the field of material science.

Luca Iuliano is currently a full professor of manufacturing systems at the Department of Management and Production Engineering of the Politecnico di Torino (Italy), director of the Integrated Additive Manufacturing center at Politecnico di Torino and President of the Competence Center CIM 4.0 in Italy. He is the author and co-author of two Italian books on rapid prototyping and investment casting and the author and coordinator of a handbook on foundry. He has published over 170 papers in academic journals and national and international conference proceedings. From 2007, he coordinated the first-level master course in "Manufacturing Systems" at Politecnico di Torino. From 2014, he has been a member of the technical-scientific committee of the ITS Foundation on Sustainable Aerospace/Mechatronics Mobility. From 2015, he has been the coordinator of the 2nd level master course in "Additive Manufacturing" at the Politecnico di Torino.

Abdollah Saboori is currently an assistant professor of advance materials processing at the Department of Management and Production Engineering and a member of the Integrated Additive Manufacturing Center at Politecnico di Torino. He has published over 100 papers in academic journals and national and international conference proceedings. He is an editorial board member of several international journals and a scientific committee member of several international conferences in the field of metal additive manufacturing. His research deals with the correlation between the properties of metallic materials and metal additive manufacturing processes.

